

# Suspended Sediment Erosion in Laboratory Flume Experiments

by

Katrina Muir Cornell

B.S. Earth, Atmospheric and Planetary Sciences  
Massachusetts Institute of Technology, 2006

B.S. Physics  
Massachusetts Institute of Technology, 2007

SUBMITTED TO THE DEPARTMENT OF EARTH, ATMOSPHERIC AND  
PLANETARY SCIENCES IN PARTIAL FULFILLMENT OF THE REQUIREMENTS  
FOR THE DEGREE OF

MASTER OF SCIENCE IN EARTH AND PLANETARY SCIENCES  
AT THE  
MASSACHUSETTS INSTITUTE OF TECHNOLOGY

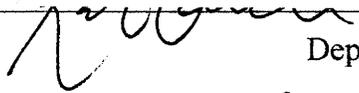
AUGUST 2007

[September 2007]

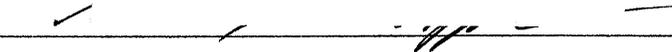
Copyright 2007 Katrina Muir Cornell. All rights reserved.

The author hereby grants to M.I.T. permission to reproduce and  
distribute publicly paper and electronic copies of this thesis document in  
whole or in part in any medium now known or hereafter created.

Author

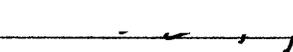
  
Department of Earth, Atmospheric and Planetary Sciences  
August 17, 2007

Certified by

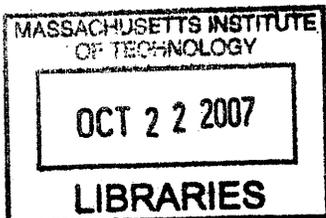


Kelin X Whipple  
Professor of Earth, Atmospheric and Planetary Sciences  
Thesis Supervisor

Accepted by



Maria Zuber  
E.A. Griswold Professor of Geophysics  
Head, Department of Earth, Atmospheric and Planetary Sciences



ARCHIVES

## **ABSTRACT**

Laboratory flume experiments are used to examine the role of suspended sediment abrasion in bedrock channel erosion. A range of topographies was used, from a planar bed to a sinuous and scalloped inner channel. Experiments were run separately with bedload (used to form topography) and suspended load at a variety of water flows and sediment fluxes. Sediment samples were collected to determine mass flux and concentration profiles. Erosion was measured between each timestep and erosion rate determined for a variety of conditions. Rouse, Froude, and Stokes numbers were calculated from measured data for various timesteps to determine mode of sediment transport and flow characteristics. Flow was supercritical, and sediment was in suspension. Erosion patterns around imposed topography perturbations (a rock protrusion and a drilled pothole) were briefly examined. A hydraulic jump was used in one timestep to see the effect of the transition from supercritical to subcritical flow. Suspended sediment causes erosion in all bed morphologies. The amount and pattern of erosion are coupled to topography, but are not constrained by it to the same degree as bedload. As in the case of bedload, suspended sediment erosion is strongly coupled to sediment flux.

## **Table of Contents**

|  |           |
|--|-----------|
| <b>Introduction</b>  | <b>5</b>  |
| <b>Experimental Method</b>                                       | <b>6</b>  |
| <b>Flume set up</b>  | <b>6</b>  |
| <b>Experimental design</b>                                       | <b>11</b> |
| <b>Data collection and analysis</b>                              | <b>14</b> |
| <b>Conditions for sediment suspension</b>                        | <b>18</b> |
| <b>Settling velocity</b>   | <b>19</b> |
| <b>Rouse number and particle suspension</b>                      | <b>20</b> |
| <b>Stokes number</b>   | <b>21</b> |
| <b>Results</b>   | <b>22</b> |
| <b>Analysis and discussion</b>                                   | <b>34</b> |
| <b>Comparison of suspended load and bedload</b>                  | <b>34</b> |
| <b>The effect of bed roughness on suspended sediment erosion</b> | <b>38</b> |
| <b>Scale of roughness</b>  | <b>39</b> |
| <b>Erosion patterns around imposed topographic perturbations</b> | <b>41</b> |
| <b>Hydraulic jump</b>  | <b>42</b> |
| <b>Comparison to previous models of suspended load erosion</b>   | <b>43</b> |
| <b>Limitations of this study</b>                                 | <b>44</b> |
| <b>Conclusion</b>  | <b>47</b> |
| <b>Appendix A – Notation</b>                                     | <b>49</b> |
| <b>References Cited</b>  | <b>50</b> |

## Figures

|  |       |
|--|-------|
| Figure1. Map of initial bed topography and slope                             | 7     |
| Figure2. Flow straightener set-up  | 9     |
| Figure3. Flume set-up for bedload runs                                       | 9     |
| Figure4. Flume set-up for suspended load runs                                | 10    |
| Figure5. Photo of hydraulic jump (e2t3)                                      | 14    |
| Figure6. Example of erosion analysis with slopemap and topography            | 16    |
| Figure7. Suspended sediment grainsize distribution                           | 17    |
| Figure8. Sediment flux ( $Q_s$ ) as a function of water flux ( $Q_w$ )       | 25    |
| Figure9. Sediment concentration profiles                                     | 27    |
| Figure10. Erosion rate (E) as a function of water flux ( $Q_w$ )             | 28    |
| Figure11. Photograph of undercut topography                                  | 30    |
| Figure12. Suspended load vs. bedload erosion in a planar bed case            | 31    |
| Figure13. Suspended load vs. bedload erosion with complex topography         | 32    |
| Figure14. Interface width (roughness) evolution                              | 32-33 |
| Figure15. Photo of pothole created with suspended sediment erosion           | 34    |
| Figure16. Location of bedload sediment in case of complex topography         | 36    |
| Figure17. Erosion rate as a function of sediment size                        | 37    |
| Figure18. Photo comparing scale of roughness with bedload vs. suspended load | 40    |
| Figure19. Photo of obstacle, erosion map                                     | 42    |
| Figure20. Local erosion of upstream faces                                    | 44    |

## Tables

|  |    |
|--|----|
| Table1. Froude numbers for suspended sediment runs     | 22 |
| Table2. Rouse numbers for suspended sediment runs      | 23 |
| Table3. Stokes numbers for suspended sediment runs     | 24 |
| Table4. Average erosion, water flow, and sediment flux | 32 |

## **Introduction**

The importance of river incision into bedrock as a driving factor in mountain range evolution and morphology is well agreed upon (Anderson, 1994; Anderson et al., 1994; Howard et al., 1994; Tucker and Slingerland, 1996; Sklar and Dietrich, 1998; Whipple and Tucker, 1999; Whipple et al., 2000). Abrasion, from grain interaction with the river bed by both suspended load and bedload, makes up one key process of bedrock channel erosion and tends to be the dominant process in streams where the bed consists of poorly jointed, massive rock (Whipple et al., 2000). The relative contributions of suspended load and bedload in channel erosion are not well constrained. Suspended load is a larger fraction of the total mass sediment flux (generally 80-90 %), but the suspended load interacts with the bed less frequently and the viscosity of water combined with the small size of much of the suspended load means impacts velocities may be reduced by viscous damping (Joseph et al., 2001)).

Infrequent, unpredictable flood events and long erosion timescales contribute to the difficulty of collecting quantitative field measurements necessary for understanding the processes at work in bedrock channel erosion. Laboratory models are a good complement to current numerical models and field studies, providing a more controlled setting and a higher density of data that allows direct quantification of active processes that can lead to enhanced physical understanding. Current models focus primarily on bedload saltation/abrasion, or assume highly simplified channel bed morphologies that downplay the importance of suspended load erosion. The Sklar and Dietrich (1998; 2001; Sklar, 2003) model of erosion addresses only the specific case of planar bed. In this model the suspended load will not interact at all with the bed, but field observations

indicate suspended load abrasion can play a part in shaping channel morphology (Hancock et al. 1998; Whipple et al., 2000; Hartshorn et al., 2002; Springer and Wohl, 2002; and reviewed by Whipple, 2004). An updated model by Lamb, Dietrich, and Sklar (in preparation) indicates near-bed suspended load may contribute to erosion, but again only the case of a planar bed is treated. Turbulence on the downstream side of obstructions and vortex currents caused by irregularities, such as flutes or potholes, focus abrasion by causing some part of the suspended load to impact the rock surface (Whipple et al., 2000). A positive feedback can develop if the nature of the suspended sediment abrasion is coupled to the bed morphology (Baker, 1974; Wohl, 1993; Wohl and Ikeda, 1997; Hancock et al., 1998; Wohl et al. 1999; Whipple et al., 2000a; and reviewed by Whipple, 2004). The parameters that govern erosion rate differ for suspended load and bedload, so knowledge of their relative roles is important in understanding landscape evolution (Hancock et al., 1998; Whipple et al., 2000).

## **Experimental method**

### **Flume Set up**

Experiments were run in an open channel flume 30 cm wide and 4 m long. The Plexiglas structure was filled with a homemade sandy cement mixture (15:1 by weight mix of sand (Sil-co-sil F110: D50 120  $\mu\text{m}$ ) to cement (Portland type 3)) that served as an erodible artificial rock bed. A strength test remains to be done, but on a batch made in preliminary studies with the same recipe the 3 tensile strengths for 6 different cores were 0.21 MPa, 0.30 MPa, and 0.24 MPa for a fully cured, damp batch. Tests done on a different, slightly less cured but dry batch gave 0.45 MPa, 0.45 MPa, and 0.51 MPa even though we expected it to be lower, so there is some variability in strengths. Whatever the

exact tensile strength, the artificial rock used here is at the weak end of the range studied by Sklar and Dietrich (2001). The cement was cured within the flume.

The bed was initially approximately planar. Erosion of channel walls was not examined in this study. The average slope of the Plexiglas base was 0.0744. The actual slope of the bed was somewhat less than that of the Plexiglas base and varied from 0.05-0.075 over the section of the flume analyzed. The irregularities were caused by imperfections in pouring technique (see Figure 1 for initial bed topography and bed slopes).

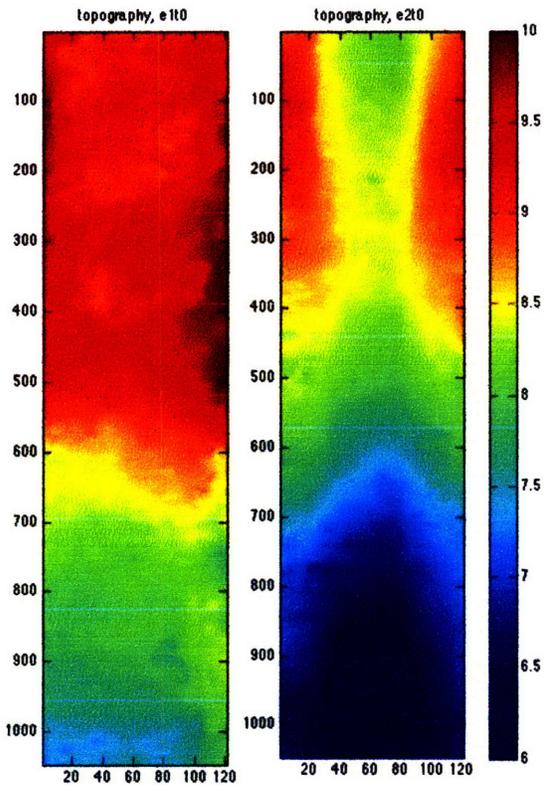
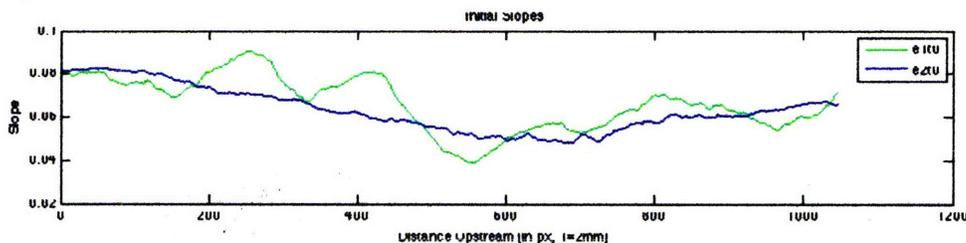


**Figure 1.** a) Initial topography of Experiment 1 (upstream end at the bottom). b) Initial topography of Experiment 2 (upstream end at the bottom). Both are on the same elevation scale, with 0 set as the Plexiglas bed and the color bar ranging from 6 to 10 cm. Notice that Experiment 2 has a topographic low down the center of the flume. c) Slope in the downstream direction of the uneroded bed for each of the two experiments for the section of the flume where erosion was measured. Green line is from initial topography of Experiment 1, blue line from Experiment 2. Slopes were calculated by averaging the elevation across the width and finding the slope of this mean elevation using the pixel spacing (2 mm). The upstream end is to the right. Axes in all three images are in pixels with 1pixel = 2 mm.

a)

b)



c)

The flume was configured to run two complete experiments using a single batch of concrete. The Plexiglas frame was designed to be twice the width necessary for one experiment and had a central Plexiglas divider. This ensured that the substrate was identical for the two experiments, and the initial conditions were very similar. There were some difficulties, however. In an attempt to create as planar a surface as possible (and to remove a hard layer that formed at the top as the cement cured) we ground down the surface. A small amount of water flowed down the side not in use. Combined with our grinding this seemed to create a soft layer at the top for Experiment 2 that probably enhanced the erosion rate in the first one or two timesteps of that experiment, as discussed in detail later. The mixture was not as homogeneous as we had hoped, and contained small (2-4 mm), hard nodules of cement within the sandy matrix. In addition, some layering of harder and weaker units (1-2 mm) thick developed during the pouring process. This layering became especially apparent in the downstream end of Experiment 2 and lead to locally severe undercutting. Consequently, this section of the flume was ignored in the analysis. We blocked the flow out of the head box for the side not in use. The opening from the headbox was slightly smaller than the width of the flume and this set up macro-turbulence structures, eddy effects, and cross currents. In order to minimize these effects we used a flow straightener over a plate of size-ordered objects (see Figure 2).

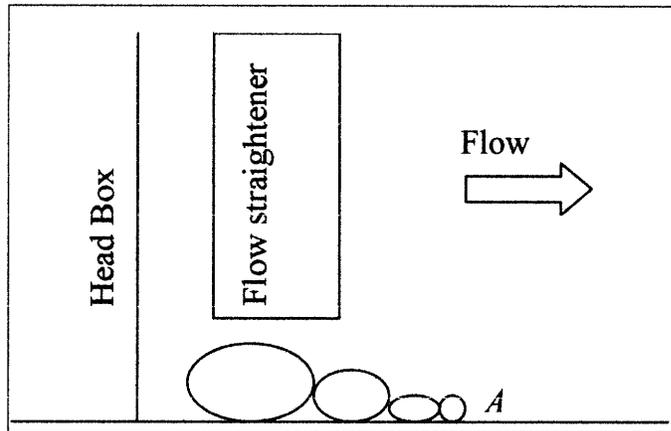


**Figure 2.** The flow straightener is a honeycomb array of circular openings. *A* is a series of decreasing diameter rocks glued into place on the bed which covered the entire width of the flume.

When using bedload, water and sediment were fed into the flume at controlled rates with the sediment collected again at the bottom before the water returned to the pump (Figure 3).

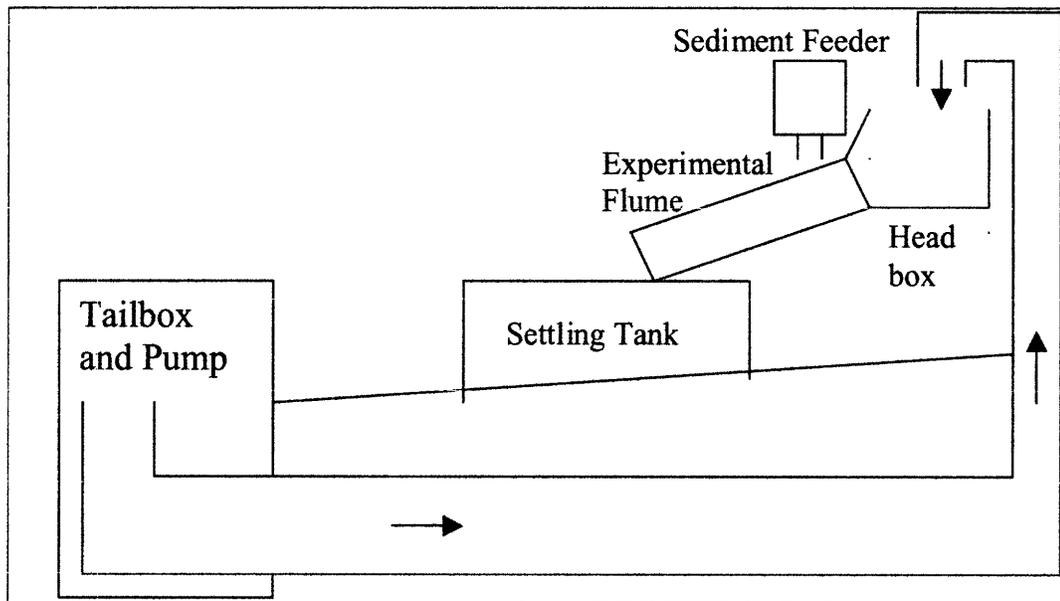


**Figure 3.** Flume set-up for bedload runs. A settling tank collected all the sediment, which was then returned to the sediment feeder manually.

Water discharge was adjustable from 0 to 80 L/s, and bedload sediment feed rate from 0-200 g/s. Two separate grain sizes were used, “2.5 mm” (D10: 2.07 mm, D50: 2.65 mm, D90: 3.22 mm) and “5 mm” (D10: 4.2 mm, D50: 5.5 mm, D90: 6.5 mm). There was no

fraction suspended load included, and all of the sediment was captured at the downstream end. Most of these results are not discussed here (Johnson and Whipple, in preparation).

For timesteps exploring abrasion by suspended sediment, sand (D10: 170  $\mu\text{m}$ , D50: 350  $\mu\text{m}$ , D90: 750  $\mu\text{m}$ , see Figure 7 (below) for full grainsize distribution) was allowed to recirculate with the water (Figure 4)

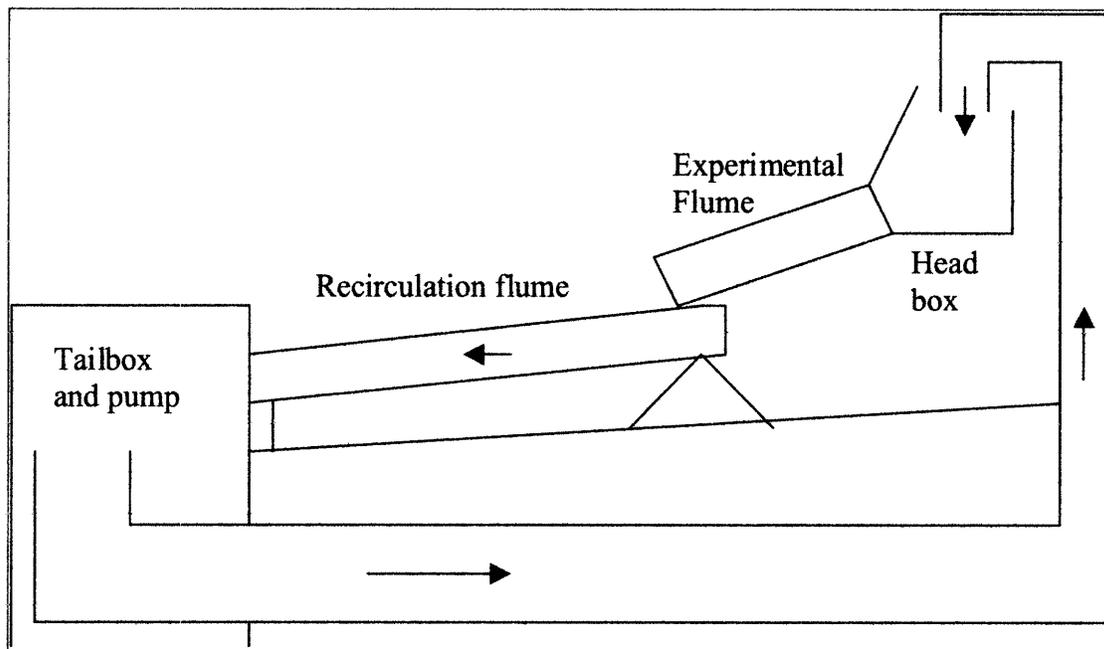


**Figure 4.** Flume set-up for suspended sediment runs. The lower flume carried the sand to the tailbox without allowing it to settle out. It then traveled through the pump, the pipe, and back into the headbox with the water. This prevented us from controlling sediment flux ( $Q_s$ ) directly, but  $Q_s$  remained dependant upon water flux, among other factors.

Although this prevented direct control of sediment concentration and sediment flux, sediment samples were taken in order to determine mass flux at various water discharges. Water flux (and therefore sediment flux) was varied, with  $Q_w$  spanning a range of 30 L/s to 80 L/s. Using Equation 1 to calculate Froude numbers for each run, it can be shown that the flow was supercritical ( $Fr > 1$ ) for all suspended load timesteps (see Table 1 in Results section for flow depth and velocity and their corresponding Froude number values).

## **Experimental Design**

In these experiments, we wished to study relationships between riverbed topography and the erosion rates and patterns of abrasion by suspended load. Despite the fact that abrasion is a key process of bedrock channel erosion, the relative contributions of abrasion by suspended load and bedload remain poorly constrained. Concurrently with these experiments, Johnson and Whipple were conducting a study of abrasion by bedload at high transport stage. In order to efficiently study both processes and to explore each under a range of bed morphologies, the suspended sediment runs were interspersed with bedload runs. For the purpose of the suspended sediment experiments, the bedload runs can be considered a simple mechanism to establish a range of initial bed configurations. In all, we used four different initial bed conditions in the suspended sediment experiments, ranging from a planar bed to a very rough bed with a well-developed, sinuous, and scalloped inner channel. We supplemented these experiments with a brief look at erosion patterns on two artificial roughness features: a large rock protrusion and a hand-drilled pothole.

By taking advantage of the two-sided flume setup, we were able to run two separate experiments from an initially planar bed using the same substrate. In Experiment 1, bedload (2-5 mm granules) was used first in order to form topography. It cut a discontinuous inner channel prior to the first run with suspended sediment. Bedload was replaced by suspended sand (D50 350  $\mu\text{m}$ ) starting with timestep 18. In order to ensure that enough sediment entered the system to force efficient sediment recirculation, we added sand while the pump was running. There are many areas of slack water in the system that act as sinks for some amount of sediment. Accordingly, we added enough

sand to the system to overcome this effect and establish quasi-steady recirculation. Suspended sediment continued to be used through timestep 25, with timestep 26 used as a “cleaning run” to remove the sand from the pipes in preparation for subsequent bedload experiments. During suspended load runs, we occasionally emptied the water from the tank to prevent biotic material from developing. Pool chlorine was also used to keep the water clean. While draining, we caught the suspended sediment in mesh traps over the drains. The inner channel was deepened by bedload abrasion over time (t27-t44) to the point where it had reached the Plexiglas bed for much of its length. Timesteps 45-49 (the last in Experiment 1) were again run with suspended sediment.

The suspended sediment flume setup was retained for the first five timesteps of Experiment 2 to observe erosion from a planar bed. Subsequently, bedload was again used to form an inner channel, but it did not cut through to the Plexiglas bed. At the end of Experiment 2 (timesteps 35 and 36), suspended sediment was revisited a final time.

In Experiment 1, a pothole (approximately 4 cm in diameter) was drilled 80 cm from the downstream end of the flume, slightly off center to the right. The timestep 6 scan shows the addition of this feature with no actual erosion (no water was run between scan 5 and scan 6). Because the conditions for the initiation of natural potholes are poorly understood, we had no guarantee one would form during the course of our experiments. Field observations indicate that the presence of potholes in natural streams is often accompanied by a dramatic increase in local erosion rates. Not all potholes reach this ideal for rapid erosion by the available tools, with some never progressing farther than a slight depression. We wanted to take advantage of our laboratory setup to study these features, though they were not the focus of this experiment. We drilled the pothole

downstream of the section of the bed used to determine erosion rates. Since the flow was supercritical, there were no upstream effects from this feature. It is entirely possible that our artificial pothole was not a best fit with the sediment available, but it still seemed a useful exercise with no ill effects on the rest of the experiment.

Also during Experiment 1 timestep 6 (e1t6), an obstacle (approximately 4 x 7 cm at the base, 2.5 cm high) made of bed material was screwed into the bed. This protrusion was again an attempt at recreating roughness that is commonly observed in the field (large boulders, for instance) to observe how the flow of water and sediment would react to the protuberance. We hoped to see erosion on the downstream face as is commonly observed in the field, but it became clear that this would not occur in the regime of supercritical flow (this is explained in greater detail later).

Experiment 2 timestep 3 (e2t3) was a suspended sediment run with a hydraulic jump. A board clamped onto the downstream end of the flume blocked some of the water and created a region of subcritical flow. Upstream of the jump the flow remained supercritical. The Plexiglas wall of the flume allowed a clear cross-sectional view of the turbulence structures at the jump. The shear layer was easily visible, and eddies were highlighted by air trapped in the flow. Figure 5 shows a photograph of the jump, with some turbulence structures drawn in.

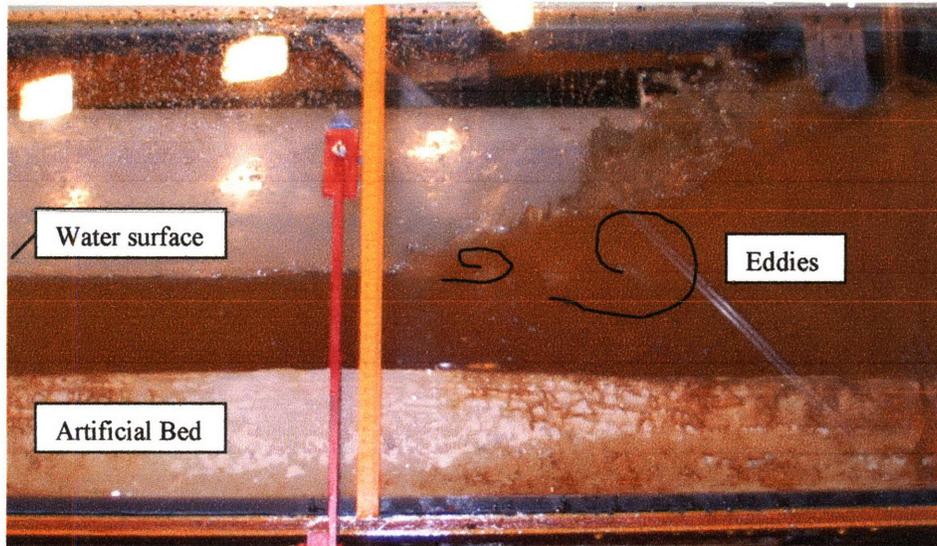


**Figure 5.** Cross-section of hydraulic jump in run e2ts3. Flow is to the right. Upstream of the jump flow is supercritical, downstream it transitions into subcritical. Turbulence structures are visible and grow to the in the downstream direction.

### **Data Collection and Analysis Methods**

Between each timestep (and after any artificial alteration of the bed) topography was measured to within  $\pm 100 \mu\text{m}$  vertical elevation with a Keyence LK-503 distance laser. Elevation data points were taken in a grid with 2 mm spacing intervals across the width of the flume and 5 mm spacing intervals in the streamwise direction (the data was interpolated to 2 x 2 mm pixel size for analysis). The laser is unable to see undercut areas and the resolution of specific features is limited by the grid spacing, so stereo photographs of the bed were taken between each timestep as a means of comparing the digital topography map to a meaningful image. The elevation data was imported into Matlab. Some corrections were necessary due to variations in the laser. The walls of the flume and specially designed targets were used as reference points to help remove long wavelength variations that appear to have been caused by changing temperature and light conditions combined with the drying of the bed surface over the course of the scan. In all images created from the scans, the direction of flow is from the bottom to the top.

Erosion maps were created for each timestep by subtracting the measured topography from that of the previous timestep. To calculate a mean erosion rate, the central section of the bed (approximately 24 cm wide) was used in all cases, removing the walls and targets. In the streamwise direction, a 2.09 m stretch of the bed starting 0.9 m from the downstream end of the flume was used for all calculations in both Experiment 1 and 2. The portion of the bed scanned began below the flow straighteners, 3 m from the downstream end, and continued to the downstream end of the flume. In Experiment 1, the erosion rates for the downstream 0.9 m of the flume (containing the pothole and protrusion) was treated separately, and in Experiment 2 it was ignored for the purpose of data analysis. A large crack through the cement on both sides of the flume formed during the first suspended sediment runs in Experiment 1. Subsequent shifting of the downstream block caused difficulty in meaningfully comparing the laser scans of sequential timesteps. In addition, a particularly hard layer at the downstream end caused unusual erosion patterns and severe undercutting (as much as 5 cm) which made accurate erosion calculations from topography impossible.

Some points were removed before averaging the erosion values. As the topography evolved, some areas (such as the walls of the inner channel) became extremely steep. Small offsets in xy position resulted in large variations in elevation measurements, which were difficult to fully correct. A slope map was created for each timestep and areas of very high slope (local gradient  $> 4$  for some runs,  $> 6$  for others) were replaced with non numerical values (NaN). The choice of the cutoff slope was made visually based on how well it removed areas of false values on the sides of inner channels. Care was taken to be sure the cutoff slope was high enough to keep the less

steep upstream faces that were often the focal points of erosion (for an example, see Figure 6).

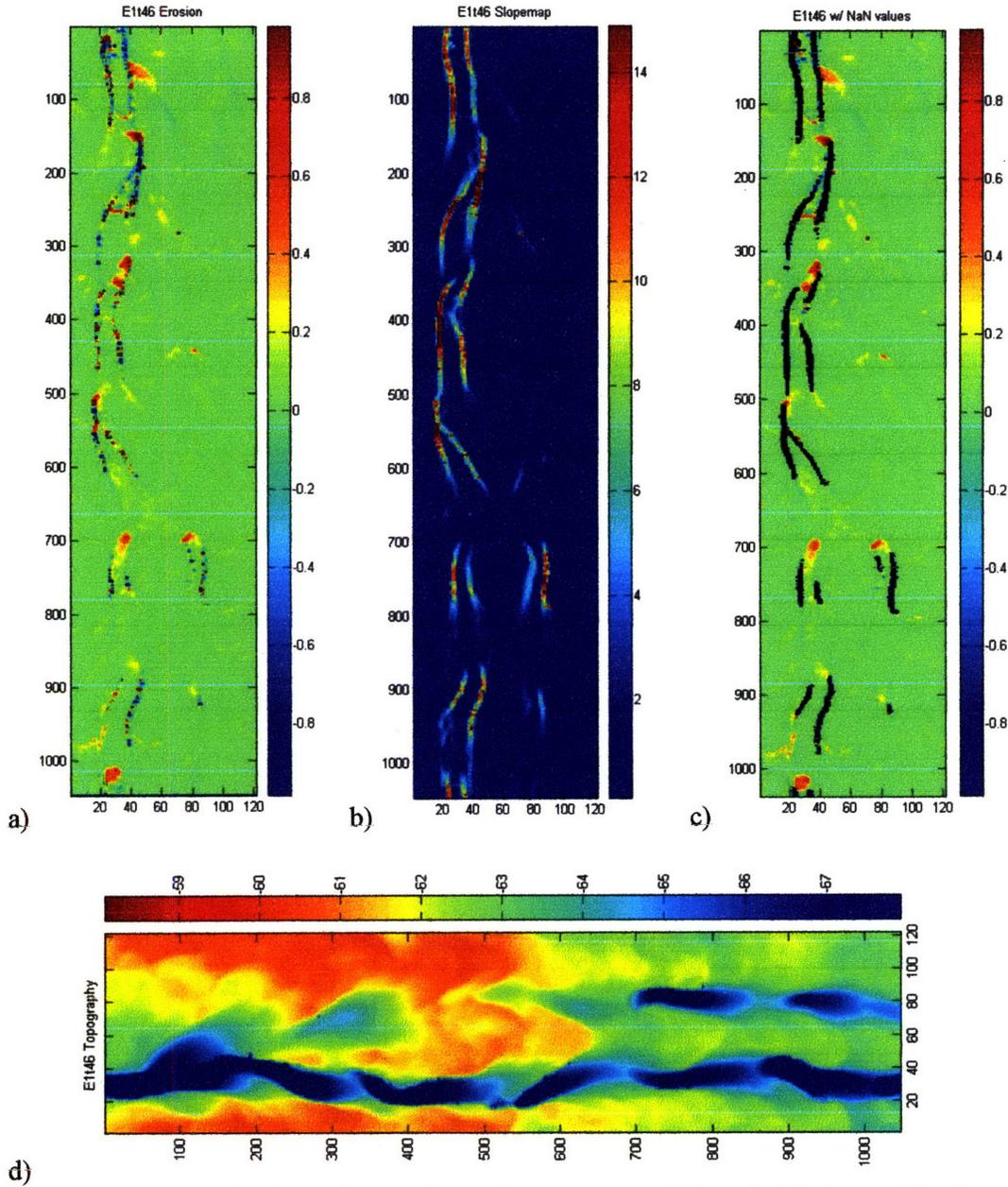


**Figure 6.** Direction of water flow is bottom to top (right to left in image d). a) Erosion map of timestep e1t46. Dots of dark blue and red along the walls of the inner channel are from errors in laser placement. b) Slope map of the timestep shows these areas have extremely high local slopes ( $> 6$ ). c) Black values cover these high slope regions, which align well with errors in image a). These values were discarded in mean erosion rate calculations. d) Topography of this run for comparison. Blues are elevation lows, reds are highs.

In addition, the laser should have an accuracy of  $\pm 100 \mu\text{m}$ , and the bed should never have aggraded (any remaining sediment was rinsed off with clean water after each timestep). For this reason, points that showed significant negative erosion were removed after the difference map was calculated but before the average erosion was found. A mean of the remaining values was calculated in Matlab.

Sediment samples were collected using a scaled-down version of the traditional Haley-Smith bedload sampler, with an opening 2.54 cm by 2.54 cm. The mesh bag caught particles above  $100 \mu\text{m}$ . The sediment was dried and weighed. Grain size distribution of each sample was measured using a Horiba CAMsizer (Retch Technology). Fitted with two digital cameras to take photographs of failing sand grains, the CAMsizer uses an elliptical projection of a particle to fit an equivalent grain volume to each grain image. Most of the particles in a sample are measured and their sizes are categorized into operator-defined size classes. For this study, the bin spacing was set to a quarter-phi interval. Figure 7 shows a sample grainsize distribution.

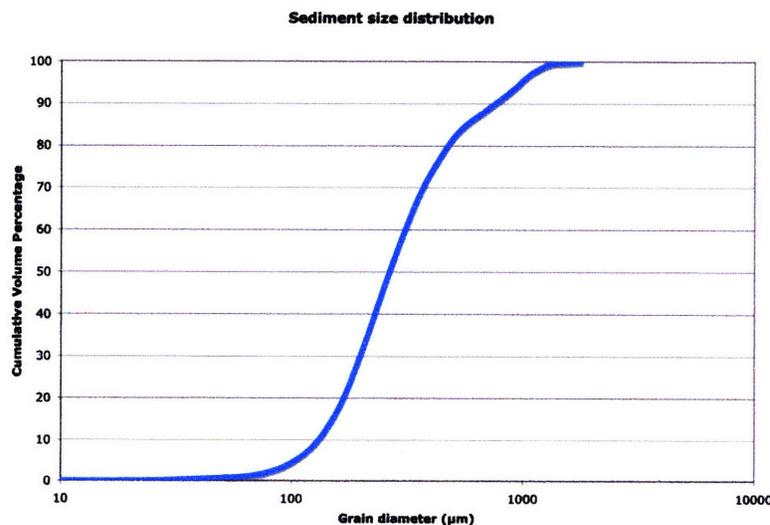


**Figure 7.** Grain size distribution of the sand used as suspended sediment in these experiments. X-axis is grain diameter (in  $\mu\text{m}$ ) on a logarithmic scale. Y-axis is cumulative volume percentage.  $D_{10} = 170 \mu\text{m}$ ,  $D_{50} = 350 \mu\text{m}$ ,  $D_{90} = 750 \mu\text{m}$ .

## Conditions for Sediment Suspension

In determining the mode of sediment transport, it is useful to calculate a few key variables. The Froude number contains information on whether the flow is subcritical ( $Fr < 1$ ) or supercritical ( $Fr > 1$ ). Froude number is defined as

$$Fr = \frac{u}{\sqrt{gh}} \quad (1)$$

Where  $u$  is the velocity of the water,  $g$  the acceleration of gravity, and  $h$  is the flow depth.

The basal shear stress,  $\tau_b$ , of the flow can be determined in a number of different ways and can vary throughout a reach depending upon local flow conditions and bed roughness. In steady, uniform flow,  $\tau_b$  can be calculated directly from the water depth and the slope.

$$\tau_b = \rho_w g h S \quad (2)$$

Where  $\rho_w$  is the density of the water,  $g$  is the acceleration of gravity,  $h$  is the water depth, and  $S$  is the reach averaged slope.

With the bed shear stress, the shear velocity can be calculated.

$$u_* = \sqrt{\frac{\tau_b}{\rho_w}} \quad (3)$$

The shear velocity describes the strength of the turbulence that acts to suspend particles. The counter force to the turbulence is gravity acting upon the grains and causing them to settle out. The rate at which this happens in quiescent water is the settling velocity,  $w_s$ .

## Settling velocity

Ferguson and Church describe a simple method for calculating  $w_s$  in their 2004 paper. In the regime where the particle Reynolds number is less than a value of  $\sim 1$ , the resistance on falling sediment in a fluid is due to the viscous drag of the laminar flow around each grain, and Stokes law (Equation 3) holds.

$$w = \frac{RgD^2}{C_1\nu} \quad (4)$$

Here  $R$  is the relative submerged specific gravity ( $R = (\rho_s - \rho_w) / \rho_w = 1.65$  for quartz in water),  $g$  is the acceleration of gravity,  $\nu$  is kinematic viscosity ( $10^{-6}$  m<sup>2</sup>/s for water at 20° C) and  $C_1=18$  is a theoretical constant.

In contrast, large particles settle rapidly and are mainly slowed by turbulent drag. For large Reynolds number (between  $10^3$  and  $10^5$ ), this creates a constant drag coefficient.

$$w = \sqrt{\frac{4RgD}{3C_2}} \quad (5)$$

Experimental results have shown  $C_2$  to be 1 for natural grains (see review in Cheng, 1997). These two expressions describe the asymptotic limits of particle settling velocity. Combining these two equations, Ferguson and Church derive an analytical expression (Equation 5) for the settling velocity that agrees well with empirical formulas (e.g. Dietrich, 1982):

$$w_s = \frac{RgD^2}{C_1v + \sqrt{0.75C_2RgD^3}} \quad (6)$$

### **Rouse number and particle suspension**

The Rouse number,  $P$ , can be used to determine what grain sizes are suspended in a given flow. The Rouse number is the ratio of the particle settling velocity to the shear velocity.

$$P = \frac{w_s}{\kappa u_*} \quad (7)$$

Where  $\kappa$  is Von Karman's constant (0.4). A good metric for the mode of sediment transport uses the following ranges in the Rouse number (from David Mohrig, MIT class notes, 12.110):

Bedload:  $P > 2.5$

50 % Suspended:  $1.2 < P < 2.5$

100 % Suspended:  $0.8 < P < 1.2$

Wash Load:  $P < 0.8$

A table of grain sizes, flow conditions, and corresponding Rouse numbers for these experiments can be found in Results. As a brief summary of the key parameter values: All Froude numbers are greater than 1 (flow is supercritical) except in the case of the hydraulic jump, which transitions to subcritical. Rouse numbers (from D50) for the

suspended sediment runs range from 0.5 to 1.2; 10 % by volume of the sand tends to be washload, 75 % is fully suspended (this is including washload, 65 % falls between Rouse number 0.8 and 1.2), and 99.9 % has a Rouse number less than 2.5 (representing the transition from suspension to bedload).

### Stokes number

Although the large volume percentage of sediment carried in suspension in most natural systems might indicate that the total kinetic energy flux of suspended sediment is greater than that of bedload (by 2-3 orders of magnitude), viscous damping of impacts can affect the efficiency of erosion by reducing the force of grain impacts with the bed. Suspended sediment, because it is smaller in size than bedload, is expected to be more strongly affected. Particles may even fail to contact the surface at low Stokes numbers.

$$S_i = \frac{\rho_s D V_i}{9\mu} = \frac{\rho_s D V_i}{9\nu\rho_w} \quad (8)$$

Where  $\rho_s$  is sediment density,  $V_i$  impact velocity,  $\mu$  viscosity of water,  $\nu$  kinematic viscosity of water, and  $\rho_w$  water density.

Joseph et al. (2000) found that below a Stokes number of about 10, no rebound occurred after a particle collision with a surface, and this indicates that the energy transmitted was low or nonexistent and that particles below this threshold will not contribute to erosion. In addition, at Stokes numbers lower than 70, the presence of the bed or an obstacle will cause particles to decelerate before collision. Some damping is present for Stokes numbers less than 500 (Joseph et al., 2000). Damping decreases the impact velocity and thus the efficiency of erosion. In our experiments, Stokes number

ranged from 63 to 2002 for near-bed suspended sediment (within 3 mm above the bed). Thus, except for a small percentage of the washload (D10 and smaller) at the lowest flows examined, little or no damping was present.

## Results

In an absence of abrasive tools (under clear water flow conditions) no erosion occurred. Flow in the flume was supercritical (Froude number greater than 1) for all suspended load runs with the exception of the section downstream of the hydraulic jump in Experiment 2 timestep 3. Table 1 shows the Froude numbers calculated for each suspended sediment run (including the upstream section of e2t3) from the surface velocity and water depth (Equation 1). In calculating water depth, the average of the laser elevation scan for each timestep was added to the base elevation of the Plexiglas. We measured the surface height of the water relative to the Plexiglas bed. The thickness of the concrete was then subtracted from this height to find average flow depth.

**Table 1.** Froude Number: values greater than 1 represents supercritical flow.

| Run      | Surface velocity (m/s) | Water depth (m) | Froude # |
|----------|------------------------|-----------------|----------|
| e1t21    | 1.921                  | 0.04            | 3.214    |
| e1t21(b) | 1.968                  | 0.04            | 3.293    |
| e1t22    | 2.497                  | 0.07            | 2.935    |
| e1t23    | 2.180                  | 0.05            | 3.283    |
| e1t23(b) | 2.168                  | 0.05            | 3.266    |
| e1t24    | 1.976                  | 0.03            | 3.443    |
| e1t25    | 2.377                  | 0.07            | 2.935    |
| e1t46    | 2.586                  | 0.09            | 2.784    |
| e1t47    | 2.600                  | 0.10            | 2.653    |
| e1t48    | 2.233                  | 0.09            | 2.364    |
| e1t48(b) | 2.443                  | 0.09            | 2.586    |
| e1t49    | 2.270                  | 0.07            | 2.768    |
| e2t1     | 2.864                  | 0.10            | 2.845    |
| e2t2     | 2.688                  | 0.11            | 2.633    |
| e2t3     | 2.413                  | 0.07            | 2.894    |
| e2t4     | 2.406                  | 0.10            | 2.380    |
| e2t5     | 2.651                  | 0.12            | 2.461    |
| e2t36    | 2.894                  | 0.08            | 3.273    |

Table 2 shows the Rouse numbers calculated from D50 (leading to the settling velocity, Equation 6) and the bed shear stress (Equation 2). No grainsize data were taken from samples collected for timesteps e1t24 and e2t2, but the same material was used in all cases. Thus, it is expected that these runs would have similar results.

**Table 2.** Rouse Number. 100 % suspended sediment is  $0.8 > P > 1.2$  (50 % suspended is  $1.2 > P > 2.5$ ).

| run   | D50( $\mu\text{m}$ ) | Rouse # |
|-------|----------------------|---------|
| e1t19 | 240                  | 0.9     |
| e1t20 | 236                  | 0.9     |
| e1t21 | 240                  | 1.3     |
| e1t22 | 266                  | 1.0     |
| e1t23 | 192                  | 1.1     |
| e1t25 | 250                  | 1.0     |
| e1t46 | 271                  | 0.9     |
| e1t47 | 297                  | 0.9     |
| e1t48 | 273                  | 0.9     |
| e1t49 | 327                  | 1.2     |
| e2t1  | 380                  | 1.0     |
| e2t3  | 351                  | 1.0     |
| e2t4  | 392                  | 1.3     |
| e2t5  | 370                  | 1.0     |
| e2t35 | 487                  | 1.1     |
| e2t36 | 524                  | 1.1     |

At the highest flows examined here, sediment smaller than 270  $\mu\text{m}$  is washload (Rouse number  $< 0.8$ ), smaller than 590  $\mu\text{m}$  was 100 % suspended (Rouse number  $< 1.2$ ), and the transition to bedload occurs at a size of 2470  $\mu\text{m}$  (Rouse number of 2.5). At the lowest flows, washload includes sediment smaller than 100  $\mu\text{m}$ , a Rouse number of 1.2 corresponds to a sediment size of 195  $\mu\text{m}$ , and the transition to bedload occurs at a grainsize of 780  $\mu\text{m}$ . While this is close to the D90 of the sand used, it is important to note that the recirculation system played a role in ensuring all sediment traveling through the flume was suspended. For the lowest flow runs, the D90 of collected sediment

samples was ~390  $\mu\text{m}$ , well below the minimum size for to bedload transport. Sediment larger than this remained in the pipe and tailbox during these runs.

Table 3 shows calculated Stokes numbers for near-bed sediment at D10, D50 and D90 at a variety of flows and water viscosities (temperatures).

**Table 3.** Stokes numbers at various impact velocities ( $V_i$ , approximately equals near-bed flow velocities for suspended sediment), water temperatures (viscosities), and grain sizes.

|      | $V_i = 0.1$ (low flow) | $V_i = 0.3$ | $V_i = 0.6$ (high flow) |
|------|------------------------|-------------|-------------------------|
| 30°C | D50: 235               | D50: 300    | D50: 350                |
| D10  | 54                     | 176         | 379                     |
| D50  | 87                     | 335         | 780                     |
| D90  | 145                    | 636         | 1673                    |
| 35°C |                        |             |                         |
| D10  | 59                     | 194         | 417                     |
| D50  | 96                     | 368         | 859                     |
| D90  | 160                    | 700         | 1841                    |
| 39°C |                        |             |                         |
| D10  | 65                     | 210         | 454                     |
| D50  | 105                    | 400         | 934                     |
| D90  | 173                    | 761         | 2002                    |

In the case of low flow, low temperatures (early in the runs; water temperatures often began at 29° C and warmed to 39° C by the end of a suspended sediment timestep) some viscous damping will occur. In the low flow runs, D50 was measured to be ~235  $\mu\text{m}$  and D10 ~145  $\mu\text{m}$ . A Stokes number of 70 occurred under these flow conditions at a grainsize of 189  $\mu\text{m}$ , meaning that 35 % by volume of the sediment in this run initially experienced some damping. As the water warmed (reducing the viscosity), the percent of sediment affected shrank. At the end of a low-flow run, a Stokes number of 70 corresponded to a grainsize of 157  $\mu\text{m}$  (approximately 13 % of sediment was affected). Stokes numbers were calculated for near-bed flow velocities (~3 mm above the bed), which in these experiments were approximately equal to the settling velocities used by Lamb et al. (in

preparation). Higher velocities farther from the bed give Stokes numbers well above the 70 cutoff found by Joseph et al. (2000).

Suspended sediment flux depended upon water flux (see Figure 8) with some complications. The water level in the tailbox affected the sediment flux. Low water levels in the tailbox resulted in higher sediment flux for the same  $Q_w$ , and when the water level in the tailbox was very high, sediment flux was dramatically reduced. Possible explanations are discussed later. Sediment flux was estimated from a few samples taken throughout the flow, but not all runs were sampled identically. The runs with the most complete 3D sampling array were used as benchmarks for the runs with fewer samples.

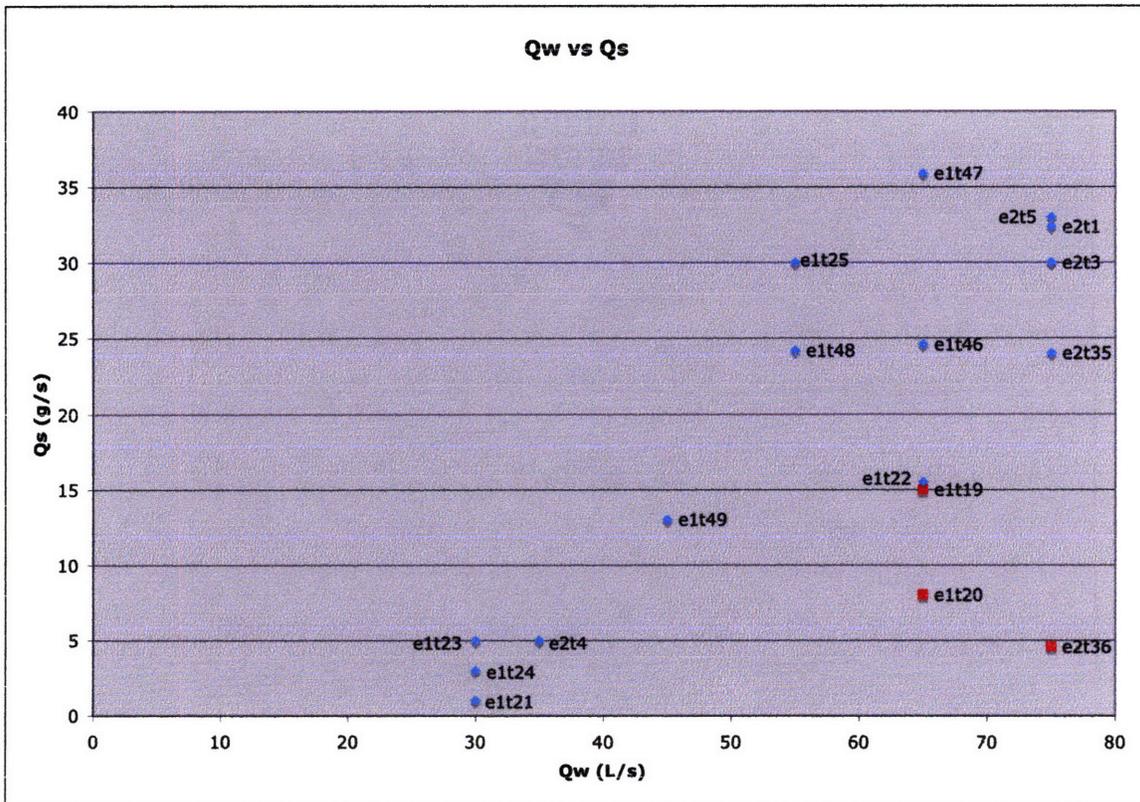
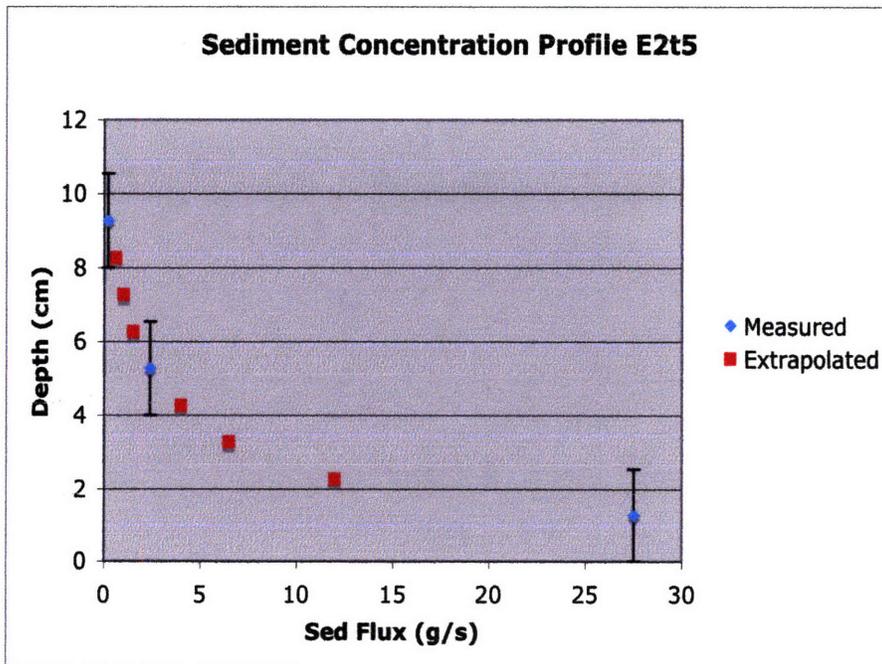


**Figure 8.** Sediment flux ( $Q_s$ ) as a function of water flux ( $Q_w$ ). E2t36 samples were taken after the tailbox was almost full of water, causing a low value. After timestep e1t20 we added additional sediment to increase the amount of material recirculating. It is expected, then, that e1t19 and e1t20 are low compared to the others. In general, it is unlikely that the sediment flux for any run is overestimated, but due to the sampling method it is possible that some points are underestimated. Given this assumption and the known low values (in red) for

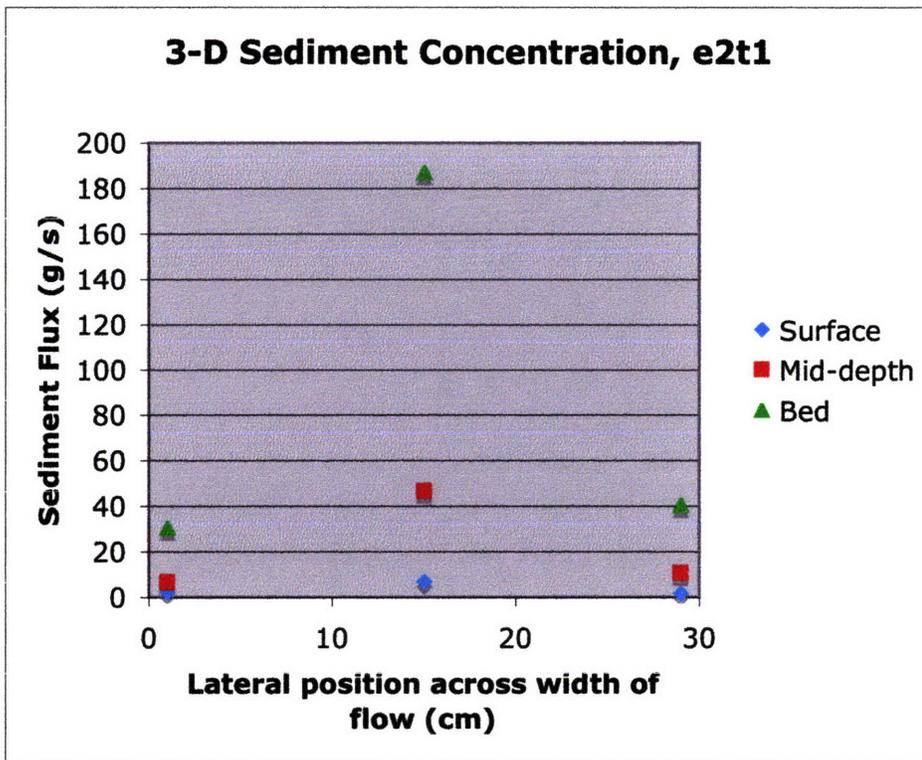
e2t36, e1t20, and e1t19, it seems the remaining values provide a nearly linear relation between sediment flux and water flux.

For the purpose of our analysis of controls on erosion rate,  $Q_w$  is used as a proxy for  $\tau_b$  and  $Q_s$ , although likely it is largely the change in  $Q_s$  that actually causes the difference in erosion.  $Q_s$  is the main control on erosion rates in the case of the bedload experiments (Johnson and Whipple, in preparation), and it is reasonable to expect that a similar relation may hold in suspended sediment erosion experiments as well. Moreover, the experimental setup allowed direct control over  $Q_w$ , and we know this value with more certainty than we know suspended sediment flux. In natural streams with plentiful sediment supply,  $Q_s$  goes as  $\tau_b^{2.5}$ . In supply-limited streams,  $Q_s$  will become constant at water fluxes above the point when the full supply of sediment is entrained.

Suspended sediment concentration is not uniform throughout the flow. Figure 9 shows a typical vertical concentration profile, and a plot of 3-D sediment concentration from e2t1.



a)



b)

**Figure 9.** a) Shows a typical sediment concentration profile, from e2t5. Blue dots are fluxes averaged over the width (for a layer 2.54 cm in the vertical) calculated from sediment samples; error bars are the size in the flow of the sediment trap. Red dots are extrapolated from these to help show the profile. b) Shows local sediment flux across the width of the flume measured from samples taken at three different depths.

The vertical profile in part a) is from samples taken in the center of the flume, but the pattern held across the full channel width, as can be seen in part b). The concentration of sediment in the center is due in part to edge effects (discussed further later), but also due to the initial bed topography of Experiment 2. The center of the flume was a topographic low, as can be seen in Figure 1.

Erosion is highly dependent upon  $Q_s$ . For the suspended sediment runs, this translates into a dependence on  $Q_w$  (from Figure 8, above). Figure 10 is a plot of Erosion rate (in mm/hr) against  $Q_w$  (in L/s).

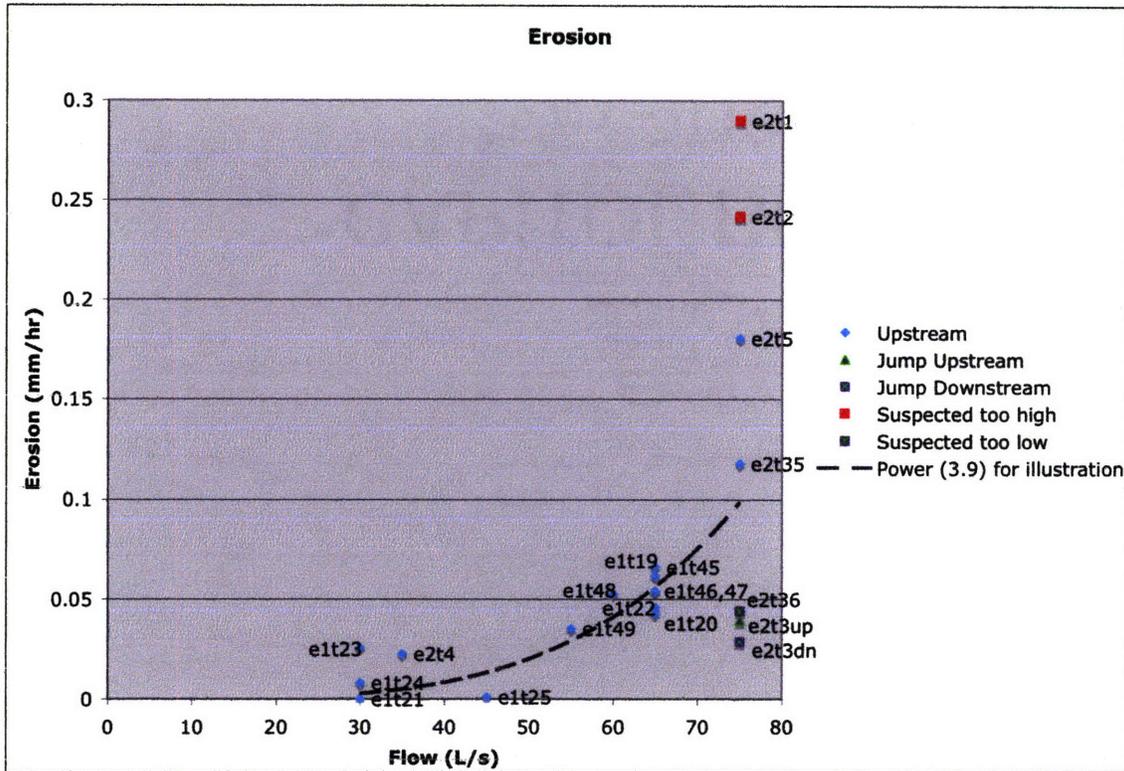


**Figure 10.** A graph of  $E$  (erosion rate, mm/hr) vs.  $Q_w$  (L/s). Values suspected to be too low are in purple, those suspected to be too high are in red. The curve (power relation with exponent 3.9) is for illustration only. E2t3 was the run containing the hydraulic jump and had much lower erosion than timesteps with similar  $Q_w$  and  $Q_s$ . E2t3 is also the only timestep that had less erosion in the downstream section than the upstream section. The downstream region of bed was contained within the subcritical part of the flow where little erosion occurred given the amount of flow and sediment recirculating. Note that for timesteps 45-49, the inner channel had cut all the way to the Plexiglas bed for much of its length. Since the suspended sediment does seem to be focused in lows (even though it is not restricted to them as observed for bedload), it is possible the erosion rates for these runs would have been higher if the Plexiglas had not stopped erosion along that section. In addition, there was a significant amount of undercutting going on in these runs, so it is likely there was more erosion than the scans show. How much more is unknown.

There are a number of factors that complicate this plot. The soft layer on the surface of the concrete at the start of Experiment 2 might contribute to high rates for the first timestep (e2t1), possibly also for the second (e2t2). E2t36 was conducted with the tailbox nearly full for part of the run. As mentioned above, this greatly reduces the amount of suspended sediment in recirculation. Since it is likely that erosion rate is more directly related to sediment concentration than water flux, it is reasonable that this point shows

markedly less erosion than might otherwise be expected from a run with high water flow. E2t3 is the run with the hydraulic jump, so the average erosion was depressed in part due to the area of subcritical flow. The inner channel had cut down to the Plexiglas bed for the late runs in Experiment 1 (e1t45-e1t49), though Figure 10 does not indicate any obvious impact of this on the relation between  $Q_w$  and E (I return to this point in the Discussion).

In addition, not all of the erosion is accounted for in the laser scan once the topography develops to the point where it becomes undercut. Figure 11 shows one example of a region with visible undercutting. At least some portion of the actual total erosion for timesteps e1t46 through e1t49 is undercutting, which cannot be recorded by the laser scanning system used.



**Figure 11.** An oblique view (looking downstream) of the bed from timestep e1t48 showing regions of undercut topography.

The pattern of erosion is partially dependent upon topography. When starting from the initially planar bed, erosion was spread broadly. Edge effects from the finite-width flume include slower flow velocity at the walls due to drag. This combines with the bed topography (the center of the flume is a topographic low) to focus a higher concentration of sediment in the center of the flume. Erosion maps for the early timesteps (no significant topography) of Experiment 2 show most of the erosion focused in the center of the channel with not much happening along the walls (e.g. Figure 12). Discounting the edge effects, erosion took place across the full width of the flume without preference to a particular location. This was true in both suspended load and bedload runs (Figure 12).

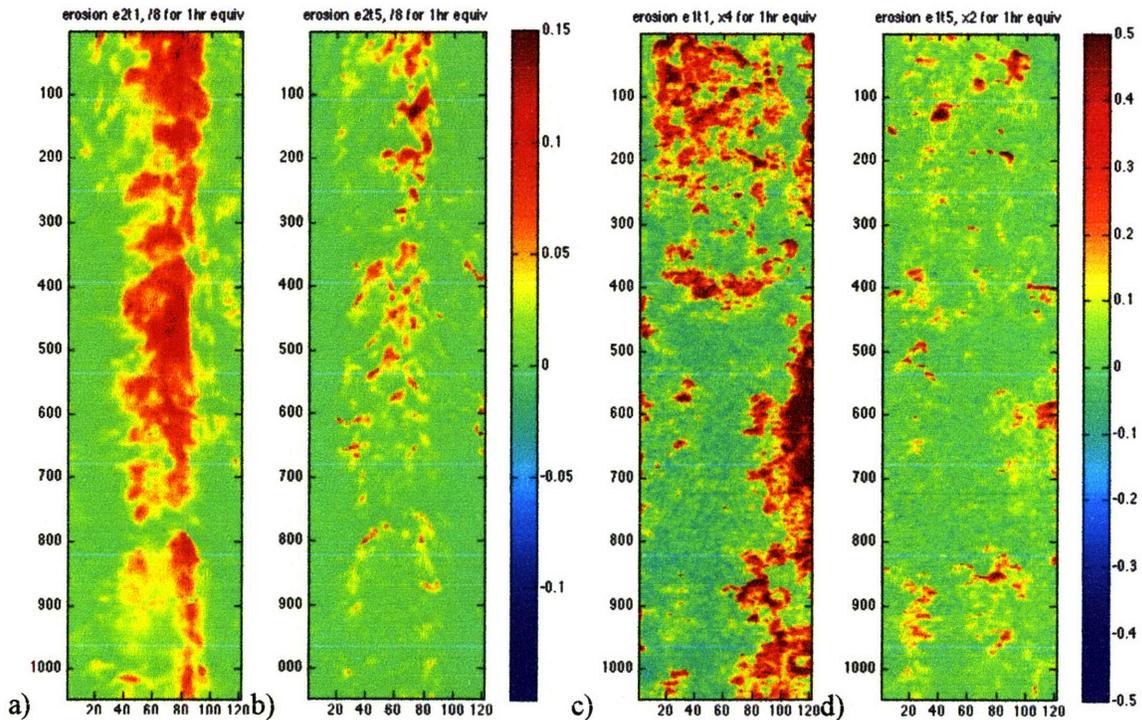


**Figure 12.** Suspended sediment vs. bedload erosion from a planar bed (no significant topography). Flow in all images is from bottom to top. All images have been corrected to show erosion rate (mm/hr) by dividing out the run time. Image a) is e2t2 (suspended load), and image b) is e2t5 (suspended load, the same run used for the sediment concentration profile above). Images a) and b) share the left colorbar and range from -0.15 cm to 0.15 cm. For comparison, image c) is e1t1 (bedload), and image d) is e1t5 (bedload). They share the right colorbar, which ranges from -0.5 cm to 0.5 cm. The lopsided nature of the

erosion towards the bottom of image c) (the upstream end) is in part due to imperfections in the sediment feeder, which were improved throughout the course of the experiments. Notice, however, that the sediment naturally spread out to fill the width of the flume in the planar bed case, so that by the downstream end this effect is no longer visible.

Once rough topography formed, the local lows focused the sediment and therefore the erosion. Despite an increased amount of erosion within the inner channel, suspended load continued to erode broadly across the width of the flume (Figure 13). This was not true in the case of bedload, which was captured more effectively by the inner channel (this result will be discussed in more detail later).

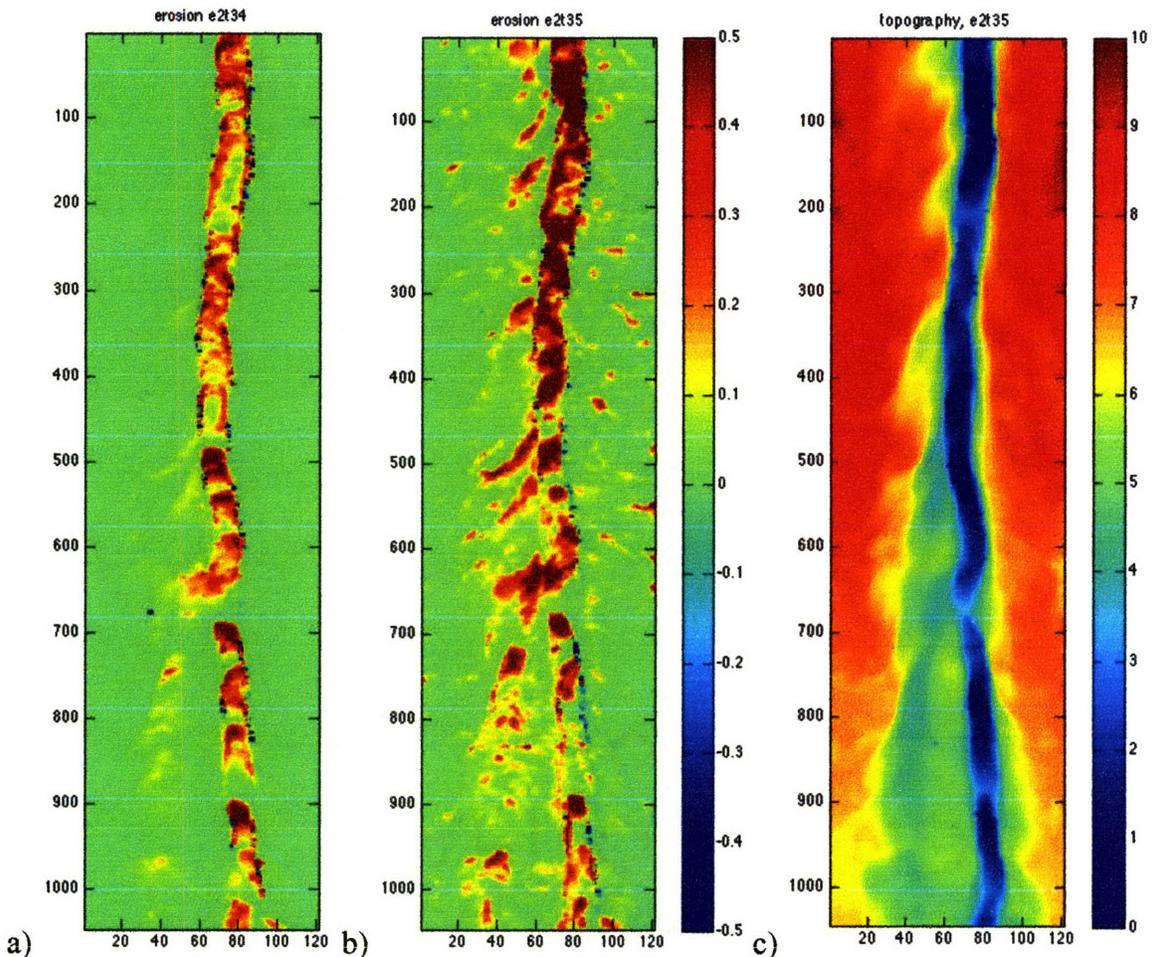


**Figure 13.** The color bars are in cm, and the axes are in pixels (1pixel = 2 mm). a) shows erosion from e2t34, a bedload run, with the erosion focused exclusively in local lows. b) is erosion from e2t35, a suspended sediment run. Erosion occurred broadly over the width, although it was higher in the topographic lows. c) is the topography for reference.

The roughness of the bed (as defined by interface width, or the ratio of the surface trace to the straight line distance across the width) increased through time as topography developed, as shown in Figure 14.

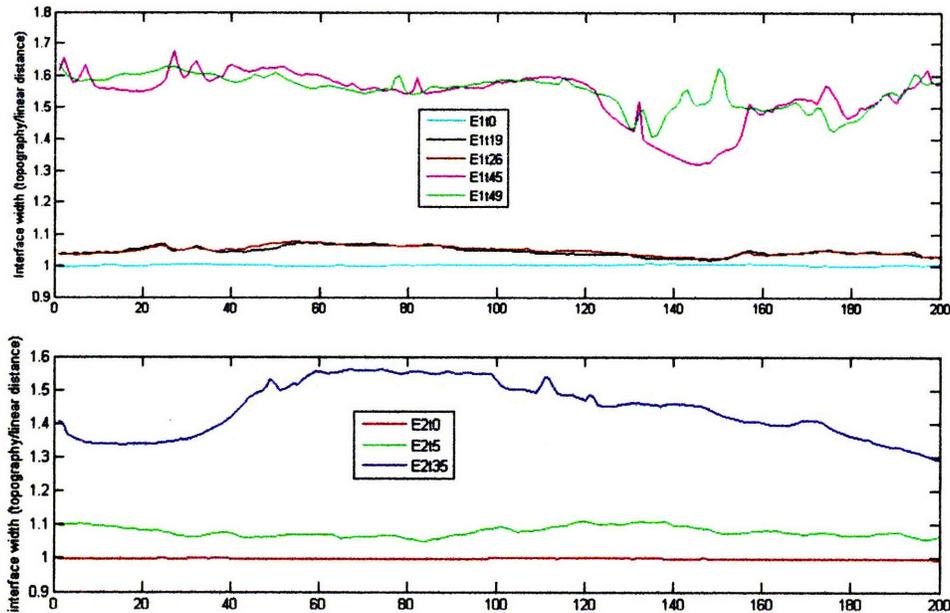


**Figure 14.** These plots show the interface width over a section of the flume. The lowest line is the planar bed (in theory should be exactly 1). Higher lines represent the start and end of each batch of suspended sediment. The top graph is for Experiment 1, the boot for Experiment 2. The x-axis is in pixels, 1 = 2 mm.

Table 4 shows the average erosion (in mm/hr) for each suspended load timestep along with the flow conditions and sediment flux (when known).

**Table 4.** Average erosion, water flow, and sediment flux for suspended sediment timesteps.

| Run   | $\sim Q_w$ (L/s) | $\sim Q_s$ (g/s) | in mm/hr |
|-------|------------------|------------------|----------|
| e1t19 | 65               | 15               | 0.07     |
| e1t20 | 65               | 8.4              | 0.04     |
| e1t21 | 30               | 1                | 0        |
| e1t22 | 65               | 15               | 0.05     |
| e1t23 | 30               | 5                | 0.03     |
| e1t24 | 30               | 3                | 0.01     |
| e1t25 | 45               | 30               | 0.001    |
| e1t45 | 65               | ---              | 0.06     |
| e1t46 | 65               | 25               | 0.05     |
| e1t47 | 65               | 36               | 0.05     |
| e1t48 | 60               | 24               | 0.05     |

|       |    |     |      |
|-------|----|-----|------|
| e1t49 | 55 | 13  | 0.04 |
| e2t1  | 75 | 32  | 0.29 |
| e2t2  | 75 | --- | 0.24 |
| e2t3  | 75 | 30  | 0.06 |
| e2t4  | 35 | 5   | 0.02 |
| e2t5  | 75 | 33  | 0.18 |
| e2t35 | 75 | 24  | 0.12 |
| e2t36 | 75 | 5   | 0.04 |

A pothole formed against the Plexiglas wall exclusively from suspended sediment erosion in runs e1t46-e1t49. Figure 15 shows a photo of the pothole from run e1t48.

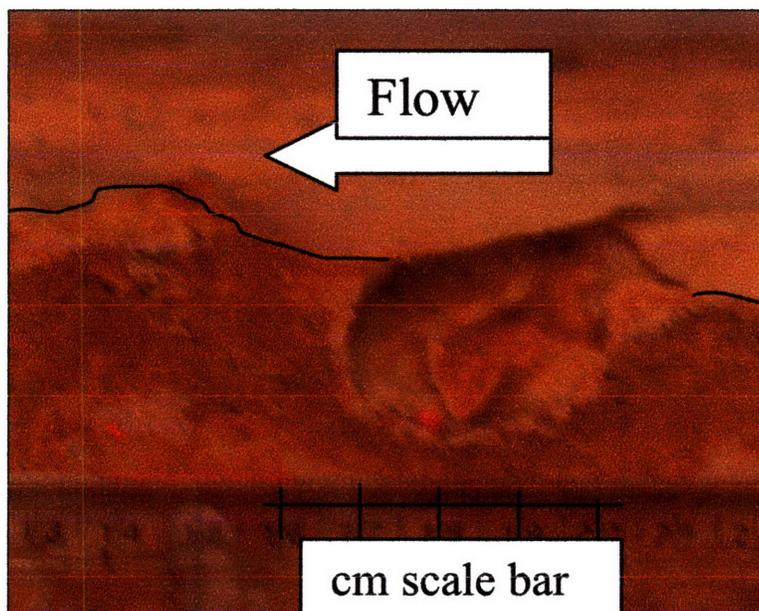


**Figure 15.** Pothole up against Plexiglas wall formed solely by suspended sediment erosion. Flow is to the left. We captured some of the erosion on high-speed video.

The pothole grew to  $\sim 4$  cm in the last four timesteps of Experiment 1. High speed video was used to examine the sediment behavior. The Rapid growth of the pothole exemplifies how local shear stress and bed topography can increase suspended sediment erosion.

## Analysis and Discussion

### Comparison of suspended load and bedload

In Figure 12, in Results, timesteps 1 and 5 from Experiment 2 (suspended load) and Experiment 1 (bedload) are placed side by side for comparison. Both cases started

from a planar bed. Because e2t1 and e2t5 were both 8-hour runs while e1t1 was 15 min and e1t5 was 30 min, the erosion data was divided by the run time to reflect an erosion rate in mm/hr. In both experiments, a planar bed resulted in erosion spread broadly over the width of the flume. The focusing of the erosion to the right on the upstream end of e1t1 was a result of uneven distribution of sediment from the feeder. We made small adjustments and continually improved the feeder to attain an even distribution of sediment upon entry to the flow. Improvement can be seen in the erosion pattern in the scan from e1t5. The sediment spread out naturally to fill the flume as can be seen by the broader erosion pattern at the downstream section. In both the case of suspended load and (to a lesser degree) bedload, the first timestep shows more erosion than later runs. This is likely an artifact of looser material at the surface-layer of cement (which, as discussed, was particularly soft in Experiment 2).

Once topography formed, it influenced the erosion. Bedload tends to travel in the local lows, causing an increase in erosion in those areas. This feedback produces the inner channel topography observed in these experiments. At some critical point, the channel is deep enough to capture all the bedload sediment and erosion of the “banks” (the rest of the bed) ceases completely. Figure 16 was created from photographic images of bedload runs. We painted the sediment red and took a series of oblique photographs at equally spaced distances down the flume. These were corrected for the oblique view, combined, and analyzed for red areas (locations of sediment). A compilation of all the photographs shows the locations where sediment was at any time during the run.

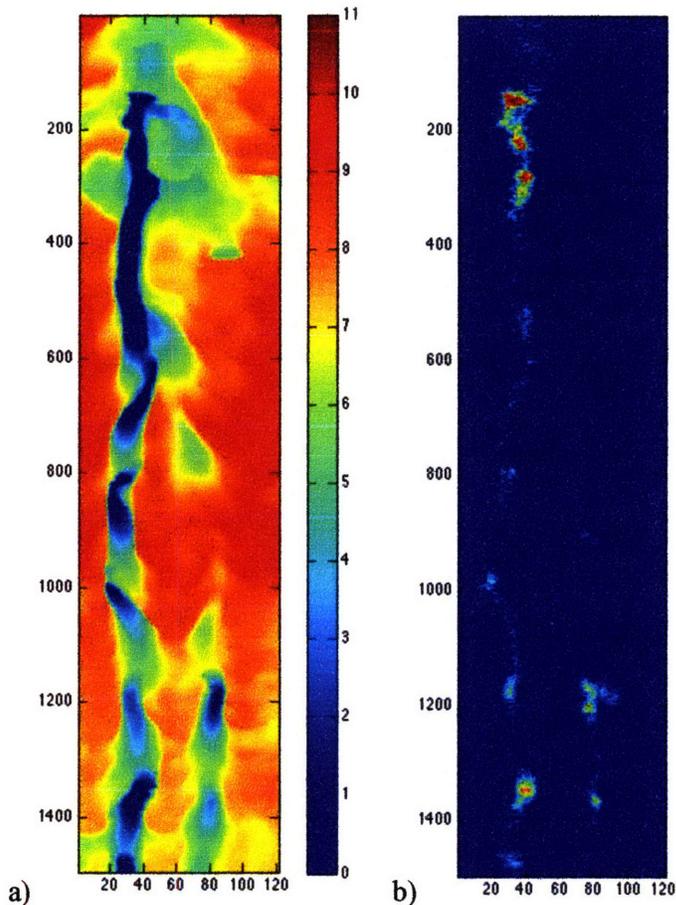


**Figure 16.** a) Topography of run e1t42, color bar in cm, 0 is the Plexiglas bed. b) Location of sediment (light blue dots show grains, brighter colors show higher concentrations). The sediment is contained within the inner channels. Notice that there is no sediment in the pothole. By the time it reaches that point, it has been entirely captured by the channel.

There is no bedload in the pothole in this run because it has all been captured by the inner channel.

Suspended sediment was not constrained in this manner. Although erosion was focused in the channel (especially on the upstream faces of its many scallops), erosion continued to take place across the rest of the bed (refer to Figure 13 from Results).

Suspended sediment caused less erosion than bedload for the same sediment flux and water flow conditions by a factor of 2-2.5. Although we did not do a direct comparison with identical conditions, Johnson and Whipple (in preparation) examined erosion rates of bedload at various  $Q_s$  while at constant  $Q_w$ . From the results of the

bedload runs of these experiments, it was determined that a comparison can be made between runs with bedload at 100 g/s and suspended load at 30 g/s by dividing the total bedload erosion rate by a factor of 2 or 3. Figure 17 shows this comparison with suspended load, 2.5 mm bedload, and 5 mm bedload.

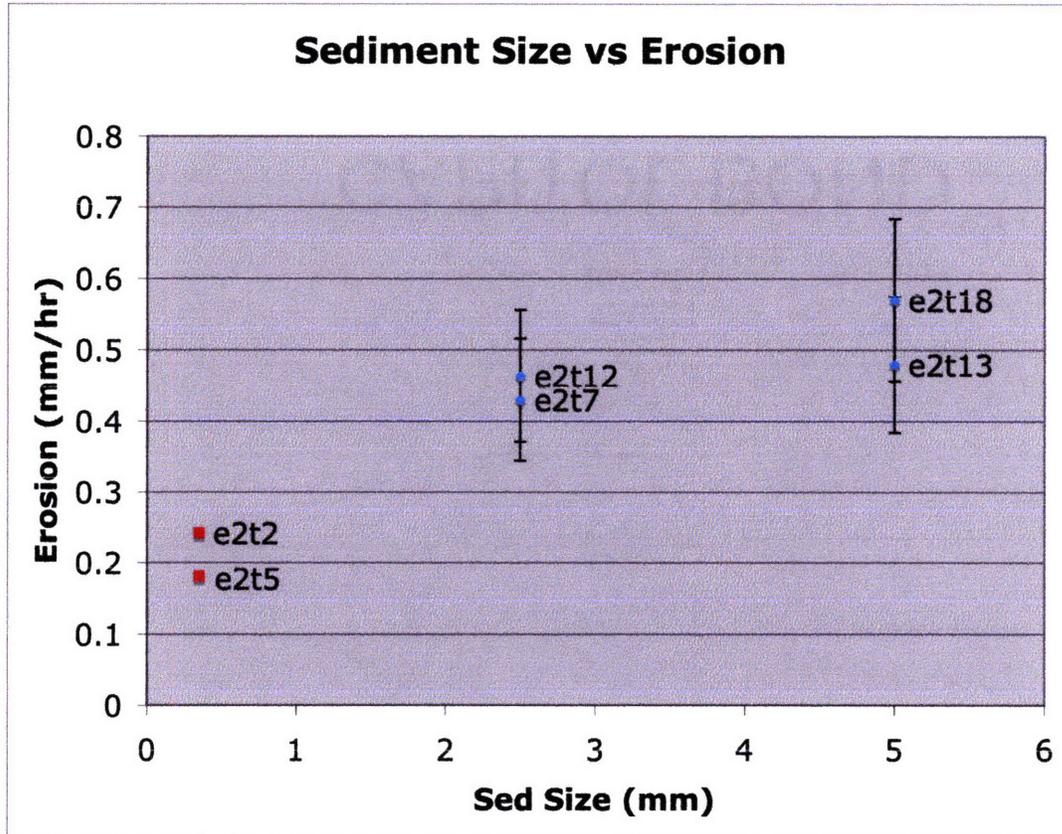


**Figure 17.** Erosion rate versus sediment size. The red squares represent two runs with suspended sediment, while the blue diamonds are four runs with bedload, two at 2.5 mm and two at 5 mm. All the bedload runs were conducted at 100 g/s sediment flux, but the suspended load was at ~30 g/s sediment flux. To correct for this, a plot of erosion rate vs. sediment flux (Johnson and Whipple, in preparation) was used. To reach the correct regime, the bedload erosion rates were divided by 2-3. The error bars represent this spread (the highest value would be dividing by 2, the lowest would be dividing by 3).

The erosion rate of suspended sediment is a bit lower than can be accounted for exclusively by its smaller size. The portion in suspension high in the flow and the part of the mass flux that is washload do not contribute to the erosion and so can account for some of this lowering. Although the erosion rates due to suspended sediment are much

lower than those due to bedload, they are still significant. In natural rivers, most of the sediment carried is thought to be suspended. Therefore, the contribution of suspended sediment to erosion might be important. In natural streams, suspended sediment might represent a larger fraction of the total erosion than the rates we found imply.

### **The effect of bed roughness on suspended sediment erosion**

As mentioned previously, the uppermost layer of concrete at the start of Experiment 2 was unusually soft (in part due to scraping of the bed in attempt to make a planar surface). This softness probably contributed to an unexpectedly high amount of erosion for a planar bed condition. Nonetheless, it still appears that roughness (as defined by interface width, or the total surface distance divided by the flume width) plays a role in the magnitude of suspended sediment erosion. There is a significant increase in erosion at the downstream end of the flume where the roughness is greater. In both runs, the majority of the undercut sections were in the downstream half of the flume. This seems to indicate that suspended load will be more effective at eroding complex bed topography than a planar bed. This result is complicated, however, and is likely due to a combination of slightly steeper bed slope in the region (imperfection in pouring technique), increased roughness, complications from the fractures that formed and grew after  $t=20$ , and possibly something inherent in the concrete and the method in which it set (with more water covering the downstream end than the upstream end, for example).

The final runs of Experiment 1 (timesteps 45-49) contain an inner channel that had cut down to the Plexiglas at its bed. It is interesting to note that the erosion values for these timesteps were very similar to those of timesteps 19-25 where the channel had not yet reached the Plexiglas. Perhaps the increased roughness of the channel in the later runs

caused an increase in erosion that was counteracted to some extent by an inability to erode further than the Plexiglas bed. In addition, undercutting was much more prevalent in the later timesteps. The material removed by this process was not accounted for in the erosion totals because the laser was unable to see those changes in bed topography. Thus, the actual erosion for timesteps 45-49 was likely higher than measured and should have been higher still had it not been impeded by the Plexiglas bed.

Increased turbulence from the bed topography might affect suspended sediment and erosion, but it is difficult to conclude anything meaningful from these results. It is possible that the roughness of the bed changed the suspended sediment concentration profile. A detailed 3-D array of suspended sediment concentration was not collected at the downstream end over the course of the bed evolution. These data would be necessary to test the hypothesis of this coupling. Increased turbulence from the bed topography may have reduced near bed sediment concentration, carrying it higher in the flow. It is, also, possible that this same turbulence would increase local erosion, so the net effect cannot be determined without further experimentation.

### **Scale of roughness**

The scale of the bed roughness, observed visually but unmeasured, appears to be related directly to the size of the tools (sediment). The scale of erosional features is most likely limited by the substrate as well, but in these experiments the smallest sediment used was still larger than the mean grain size of the cement, so we did not observe that limitation.

Erosion by sand (the suspended sediment used in these runs) causes fine fluting and sharp angles. These delicate features are chipped out by bedload (Figure 18).

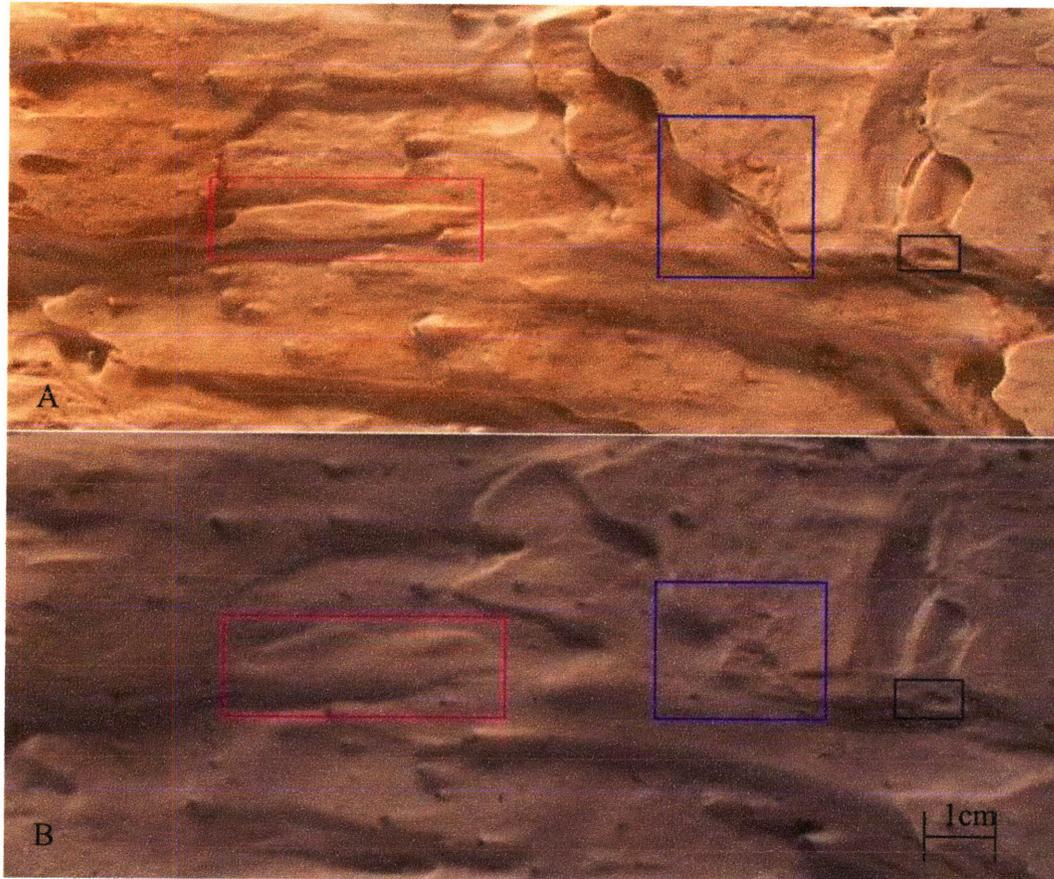


**Figure 18.** Photo A is after run e1t20, just two runs of suspended sediment photo B is after run e1t15 of the same section of the bed. Notice how the topography is smoothed out in photo B.

A general size of the grooves and features that formed on the bed, also, seemed to vary between the 2.5 mm bedload sediment and the 5 mm bedload sediment. The level of detail necessary to gain quantitative information about this observation is not visible in the laser scans which took points every 2 mm across the width and every 5 mm in the streamwise direction. The large-scale bed topography (the inner channel morphology) was caused by the bedload erosion. To gain a better understanding of how grainsize affects morphology, it might be necessary to run a single experiment to a complex morphology using only one grainsize (2.5 mm bedload, for example) followed by another complete experiment using a different grainsize (5 mm for example).

Larger sediment will remove features created by the smaller sediment, but only where there is enough large sediment to impact the bed with a high enough frequency to cause erosion across the width of the stream. It is likely that there would be a crossover point in a mixture of sediment sizes where the larger sediment must make up some critical percentage of the total sediment flux before the features reflect its size.

Erosional features will probably vary throughout the depth of the flow. At the bed, larger sediment will dominate the scale of roughness. Higher in the flow, where larger sediment only seldom impacts the walls or surfaces of boulders, finer sediment may dominate. Observations of erosional features might then contain information about the size and mixtures of sediment carried in a flow. Again, the resolution of information will be limited by the substrate being eroded.

It is also possible that the difference in observed erosion scales creates feedback loops where finer sediment takes advantage of fine scale roughness to create erosional features that are then large enough to be broken off by larger sediment. This would increase the total erosion rate beyond a simple addition of the different rates associated with single sediment sizes.

### **Erosion patterns around imposed topographic perturbations**

Erosion of the pothole (described in the experimental methods section) occurred in both bedload and suspended load runs. Most of the erosion took the form of undercutting on the upstream wall of the pothole, rendering it invisible to the laser scans. Bedload erosion in the pothole was maintained only until the inner channel formed. This channel captured all the bedload sediment at a point upstream of the pothole and cut off its tool supply, causing erosion in the pothole to cease. Suspended sediment did cause

some erosion in the pothole after the channel had formed, but a large part of the erosion was undercutting in the upstream direction and was not captured in the laser elevation data.

The upstream face of the obstacle (Figure 19) eroded rapidly due to the high rate of impacts and the large horizontal velocity of the particles carried in the flow.



**Figure 19.** Photos of protrusion (slightly different angles). a) Initial shape; b) after some erosion has occurred. Flow is from the left. Upstream erosion is evident; downstream face remains unchanged. c) shows the formation of horseshoe shaped flutes around the protrusion. The low to the right is the pothole. Colorbar shows elevation in cm.

No erosion occurred on the downstream face. Because of the supercritical nature of the flow, the sediment was never able to impact the downstream face of the obstacle. Rather, sediment was swept around causing a local increase in erosion and forming a set of horseshoe shaped flutes (Figure 19, c). These rapidly undercut the sides of the protrusion.

Perhaps in a condition of slower flow but larger flow volumes and high eddy velocities, sediment will be able to impact the downstream face of boulders and other obstacles to cause the erosion patterns observed in the field (Hancock et al, 1998; Whipple et al, 2000). In a laboratory setting, a larger object that effectively blocked more of the flow and forced an eddy to fill in behind would be sufficient, but we did not test this theory.

## Hydraulic Jump

The hydraulic jump of  $e^{2/3}$  described in the experimental methods section resulted in a substantial reduction of erosion at the point where the flow changed from supercritical to subcritical. The flow deepened and slowed, becoming visibly more turbulent. This was the only timestep for which the erosion in the downstream section (of 90 cm or so) was less than the upstream section.

One possible reason for this dramatic decrease in erosion in the region of subcritical flow was the significant slowing of the flow. The average kinetic energy of the sediment grains was greatly reduced as the flow that carried it slowed, and the reduction of impact velocity would translate into a reduced erosion rate. In addition, the increased turbulence may have acted to carry the near bed suspended sediment higher in the (deeper) flow, lowering the near bed concentration. Since erosion rate is highly dependent upon sediment flux, this alteration of the sediment concentration profile could reduce the erosion rate.

### **Comparison to previous models of suspended load**

The Sklar and Dietrich (1998; 2001; Sklar, 2003) model of bedrock erosion looks at the limited case of a planar bed and predicts suspended sediment will never impact the bed, and thus, it will cause no erosion. Their updated model (Lamb et al., in preparation) removes the assumption that impact rate tends to zero as the threshold of suspension is reached. They acknowledge that near-bed suspended sediment will cause some erosion, but they still examine only the case of a planar bed, where near-bed settling velocity equals the impact velocity. When a particle impacts an upstream face, however, the downstream velocity of the particle must be taken into account. Since the rate of erosion

scales with the cube of impact velocity (Lamb et al., in preparation), this is a significant effect. Figure 20 shows local erosion focused on upstream faces of bed irregularities.

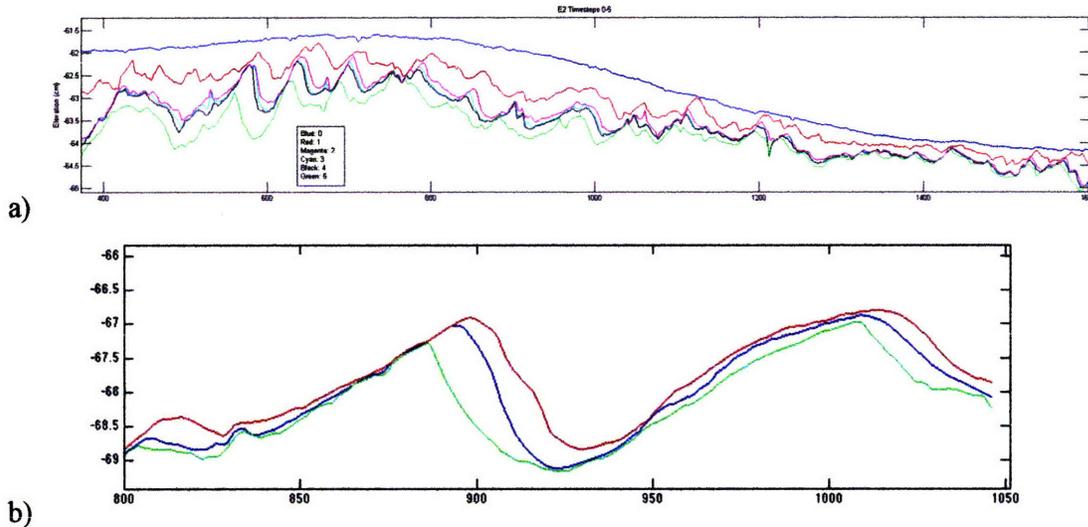


**Figure 20.** a) Streamwise topography (with large vertical exaggeration), down the approximate center of the flume over the first five timesteps of Experiment 2. Flow is to the left. Notice how much of the erosion takes place on upstream faces, while downstream faces contain practically no erosion. b) A close-up of a cross-section of the bed topography over a series of three timesteps. Flow is again from right to left. The scale bar on the y-axis is in cm, the x-axis is in pixels (1 pixel = 2 mm, 5 pixels = 1 cm)). The upstream face in the center shows the most significant erosion, while the downstream faces show almost none.

We observed this effect in both suspended load and bedload runs.

### Limitations of this study

Although we attempted to create a planar bed as the initial condition, it was not truly planar. Figure 1 shows the initial topographies of Experiments 1 and 2, and the width-averaged slope of the same.

The finer scale irregularities caused by the hard nodules of concrete within the sandy matrix served as initiation points for erosion to occur. Larger scale inhomogeneities, such as unusually hard layers, added to the complexity in interpreting the erosion data. A harder layer may have contributed to the unusually low erosion rate in

e1t25 given the flow conditions and sediment flux. Bedload was used in the next few timesteps and eroded through this layer.

Conversely, the soft layer at the top of Experiment 2 (not present to the same degree at the start of Experiment 1) makes it more difficult to examine suspended sediment erosion from a planar bed. It is likely that there would be some erosion from near bed suspended sediment even in a case of a truly planar bed with a more typical hardness, but in a reduced amount from what was observed. Experiment 1 timestep 1 is almost certainly an exaggerated amount of erosion compared to the other timesteps, and it is possible that e1t2 still showed some of these effects. E1t5 is perhaps a more accurate reflection of what can be expected.

As previously mentioned, the inner channel cut down to the Plexiglas bed during the course of these experiments, influencing the results an unknown amount. Either thicker initial concrete or more experiments of shorter duration would help prevent this from happening.

One of the biggest difficulties with our set up was the lack of a good control over suspended sediment flux. The main recirculation pipe had a large diameter and carried a higher volume of water than was traveling through the flume. Inside the pipe, the water was traveling more slowly than through the flume. Sediment that was suspended in the flume settled out in the pipe. At lower flows the sediment flux dropped off rapidly to zero, while at higher flows sediment flux was not as consistent as we had hoped. Towards the end of our experiments, we discovered that the total amount of water in the system (and therefore the level of water in the tailbox) was a significant factor in sediment recirculation. Lowering the water level caused more sediment to recirculate. It allowed

air to enter through the pump into the pipe, increasing turbulence and forcing more sand into suspension in that phase of the cycle. Partially closing the valve in this pipe seemed to contribute to increased sediment circulation, again by increasing the turbulence in the pipe. For future studies, we recommend a smaller recirculation pipe be used. This should allow more consistent sediment flux and would extend the lower range of water flows ( $Q_w$ ) over which sediment can be recirculated.

We used the sand available to us, which contained a mix of grain sizes (D10: 170 $\mu$ m, D50: 350 $\mu$ m, D90: 750 $\mu$ m). In contrast to the settling tank used for the bedload, there was no easy way to strain the sand. It was kept recirculating in the system (with associated problems) until a set of runs was completed. We were unable to examine a fine gradation of sediment sizes to see at which grain sizes maximum erosion occurs and at which critical diameter erosion ceases all together. In theory, the transition to washload seems a logical point for erosion to stop, but it might fall to negligible rates before that point is reached. After some suspended sediment runs, we drained and refilled the tank. We used mesh traps over the drains to catch most of the sediment. This made the water clearer and likely reduced the overall mass flux slightly by removing some of the washload (sediment that never interacts with the bed, Rouse # < 0.8). The near bed suspended sediment (the actively eroding fraction) should not have been affected.

In order to achieve enough erosion with suspended sediment that the differences between runs were visible, we ran the pump for 8hrs for each timestep. The heat from the pump warmed the water up (on some runs as high as 39°C). This temperature change does affect the viscosity of the water, but not a significant amount given range of Stokes numbers in most of these experiments. With the exception of the experiments with the

lowest flows, even the highest viscosities (lowest temperatures) are not enough to dampen sediment impacts. In the lowest flow case, there will be some minor damping (Stokes number ranging between 50 and 70) for up to 35 % (by volume) of the sediment. This number is reduced to 13 % by when viscosity has reached its final value at the end of the run. However, the heat may have contributed to the large cracks that formed in the downstream section of the bed, since they first appeared after a series of suspended sediment runs.

### **Conclusions**

Laboratory flume experiments are a useful method for gaining insight into natural streams in a more controlled environment. Contrary to existing models, it is clear from these experiments that suspended sediment is capable of significant abrasive erosion of bedrock, and it is therefore an important factor when considering natural bedrock channels. There is still much work to be done, however, in more precisely defining the controls of suspended sediment erosion and in examining a wider range of parameter space.

In this study, non-dimensional numbers such as the Froude number ( $Fr$ ), Rouse number ( $P$ ), and Stokes number ( $S_t$ ) were used to determine the regime of sediment transport and to gain insight into flow characteristics and sediment interaction with the bed. It was determined that flow in all timesteps was supercritical, the sand used was within the suspended regime, and viscous damping was not a significant effect.

In our set-up, sediment flux ( $Q_s$ ) was found to be approximately linear with water flux ( $Q_w$ ), allowing analysis to be done with  $Q_w$ , a more precisely measured quantity. Erosion rate was then observed to be dependant upon  $Q_w$  ( $Q_s$ ) to some power greater than

one. More precise control over sediment flux and a greater range of testable water flows could be achieved in future experiments by using a small diameter recirculation pipe. It might also be useful to examine cases of higher flow volumes and lower water velocities.

Large-scale roughness of the bed likely accentuates suspended sediment erosion by increasing local shear stress, increasing turbulence, and providing a larger surface area that covers a range of flow depths. Small-scale erosion features appear to be dependant upon grainsize. Interactions of a mix of grainsizes (both suspended load and bedload) may induce higher erosion rates than a simple sum would require.

Suspended sediment erosion is coupled to topography, but not as fully constrained by it as bedload. Even in the case of a well-defined inner channel, suspended sediment eroded across the full width of the bed. In contrast, bedload was fully captured by the inner channel. Field observations show dramatically greater erosion on the downstream faces of boulders than on the upstream faces. The protrusion created in our study displayed the opposite effect, with erosion only occurring on the upstream face.

## Appendix A – Notation

|          |   |
|----------|---|
| $C_d$    | Drag coefficients (dimensionless)             |
| $D$      | Sediment diameter (L)                         |
| $E$      | Rate of vertical erosion ( $LT^{-1}$ )        |
| $Fr$     | Froude number (dimensionless)                 |
| $g$      | Acceleration due to gravity ( $LT^{-2}$ )     |
| $h$      | Depth of flow (L)                             |
| $P$      | Rouse parameter (dimensionless)               |
| $Q_s$    | Sediment flux ( $MT^{-1}$ )                   |
| $Q_w$    | Water flux ( $VT^{-1}$ )                      |
| $R$      | Submerged specific density of sediment        |
| $Re$     | Reynolds number (dimensionless)               |
| $S$      | Slope (dimensionless—L/L)                     |
| $S_t$    | Stokes number (dimensionless)                 |
| $u$      | Streamwise velocity of water                  |
| $u_*$    | Shear velocity ( $LT^{-1}$ )                  |
| $V_i$    | Impact velocity ( $LT^{-1}$ )                 |
| $w_s, w$ | Settling velocity of a particle ( $LT^{-1}$ ) |
| $\kappa$ | von Karman's constant                         |
| $\mu$    | Viscosity                                     |
| $\nu$    | Kinematic viscosity                           |
| $\rho_s$ | Density of sediment ( $ML^{-3}$ )             |
| $\rho_w$ | Density of water ( $ML^{-3}$ )                |
| $\tau_b$ | Basal shear stress ( $ML^{-1}T^{-1}$ )        |

## References Cited

- Anderson, R.S., 1994, The growth and decay of the Santa Cruz Mountains: *Journal of Geophysical Research*, v. 99, p. 20161-20180.
- Anderson, R. S., Dick, G. S., and Densmore, A., 1994, Sediment Fluxes from model and real bedrock-channeled catchments: Responses to baselevel, knickpoint and channel network evolution: *Geological Society of America Abstracts with Programs*, v. 26, no. 7, p. 1270-1278.
- Baker, V., 1974, Erosional forms and processes from the catastrophic Pleistocene Missoula floods in eastern Washinton, *in* Morisawa, M., ed., *Fluvial geomorphology*: London, Allen and Unwin, p. 123-148.
- Cheng, N.-S., 1997, Simplified settling velocity formula for sediment particle: *Journal of Hydraulic Engineering, American Society of Civil Engineers*, v. 123, p. 149-152.
- Ferguson, R.I., and Church, M., 2004, A simple universal equation for grain settling velocity: *Journal of Sedimentary Research*, v. 74, no. 6, p. 933-937.
- Hancock, G. S., Anderson, R. S., Whipple, K. X., 1998, Beyond power: bedrock river incision process and form, *in* Tinker and Wohl, 1998, *Rivers Over Rock: Fluvial Processes in Bedrock Channels*, Washington, D. C>: American Geophysical Union, p.35-60
- Hartshort, K., Hovius, N., Dade, W. B., Singerland, R., 2002. Climate-driven bedrock incision in an active mountain belt: *Science*, v. 297, p. 2036-38.
- Howard, A. D., Seidl, M. A., and Dietrich, W. E., 1994, Modeling fluvial erosion on regional to continental scales: *Journal of Geophysical Research*, v. 99, p/ 13971-13986.
- Johnson, J. and Whipple K. X, in preparation. Isolating the influence of shear stress, sediment supply, and alluviation in bedrock channel incision experiments.
- Joseph, G. G., Zenit, R., Hunt, M. L., and Rosenwinkel, A. M., 2001, Particle-wall collisions in a viscous fluid: *Journal of Fluid Mechanics*, v. 433, p. 329-346.
- Mohrig, D. MIT EAPS Sedimentology class notes, fall 2004.
- Sklar, L., 2003, The influence of grain size, sediment supply, and rock strength on rates of river incision into bedrock. PhD Thesis. University of California, Berkeley. 343 pp.
- Sklar, L., and Dietrich, W. E., 1998, River longitudinal profiles and bedrock incision models: Stream power and the influence of sediment supply, *in* Tinkler, K. J., and Wohl, E. E., eds, *Rivers over rock: Fluvial processes in bedrock channels*: Washington, D.C., American Geophysical Union, p. 237-260.
- Sklar, L., and Dietrich, W. E., 2001, Sediment and rock strength controls on river incision into bedrock: *Geology* v. 29, p. 1087-90.
- Springer, G. S., and Wohl, E. E., 2002, Emperical and theoretical investigations of sculpted forms in Buckeye Creek Cave, West Virginia: *Journal of Geology*, v. 110, p. 469-481.
- Tucker, G. E., and Singerland, R., 1996, Predicting sediment fluz from fold and thrust belts: *Basin Research*, v. 8, p. 329-349.
- Whipple, K. X, 2004, Bedrock rivers and the geomorphology of active orogens: *Annual Review, Earth and Planetary Science* v. 32, p. 151-85.
- Whipple, K. X, and Tucker, G. E., 1999, Dynamics of bedrock channels in active

- orogens: Implications for height limits of mountain ranges, landscape response timescales, and research needs: *Journal of Geophysical Research*, v. 104, p. 17661-17674.
- Whipple, K. X, Hancock G. S., Anderson, R. S., 2000, River incision into bedrock: mechanics and relative efficacy of plucking, abrasion, and cavitation: *Geological Society of America Bulletin* v. 112, p 409-503.
- Wohl, E. E., 1993, Bedrock channel incision along Picanniny Creek, Australia: *Journal of Geology*, v. 101, p. 749-761.
- Wohl, E. E., and Ikeda, H., 1997, Experimental simulation of channel incision into a cohesive substrate at varying gradients: *Geology*, v. 25, p. 295-98.
- Wohl E. E., Thompson, D. M., Miller, A. J., 1999, Canyons with undulating walls: *Geological Society of America Bulletin*, v. 113, p. 1205-12